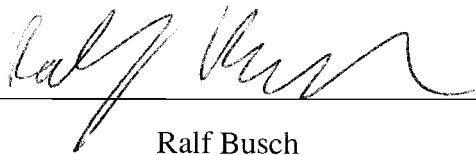AN ABSTRACT OF THE THESIS OF

Manish G. Bothara for the degree of Master of Science in Materials Science presented on November 11, 2004.

Title: Diffusion Bonding and Embossing of $Zr_{46.7}Ti_{8.3}Cu_{7.5}Ni_{10}Be_{27.5}$ Bulk Metallic Glass Forming Alloy.

Abstract approved:

_____

Ralf Busch

A Bulk Metallic Glass (BMG) is an amorphous solid with thickness greater than 1mm. Material properties of BMG, like twice the strength of regular steels and excellent corrosion resistance, make them ideal materials for fabrication of MEMS and MECS devices which have attracted a lot of research activity recently. Diffusion bonding and embossing was attempted for $Zr_{46.7}Ti_{8.3}Cu_{7.5}Ni_{10}Be_{27.5}$ (Vit4), a BMG forming alloy. Determination of experimental parameters based on material properties like viscosity and diffusivity, is discussed in this paper. To achieve embossing, various dies were pressed into the Vit4 pieces which were softened by heating them to temperatures close to or above the glass transition. Characterization of the replicated surface using an optical microscope and a surface profiler showed that a replication accuracy of 97% could be achieved successfully. Bonding of the two Vit4 pieces was facilitated by holding them at an elevated temperature for a certain time and under a certain

pressure. Differential Scanning Calorimetry (DSC) revealed that the material did not crystallize during embossing but it underwent a phase separation. Bonding was achieved for runs where Vit4 crystallized while a weak bond resulted in the run where the sample was amorphous. Thus it was concluded that Ni diffusion of more than 150 nm was required for formation of a strong bond.

Diffusion Bonding and Embossing of $Zr_{46.7}Ti_{8.3}Cu_{7.5}Ni_{10}Be_{27.5}$ Bulk Metallic Glass

Forming Alloy

by

Manish G. Bothara

A THESIS

submitted to

Oregon State University

in partial fulfillment of

the requirements for the

degree of

Master of Science

Presented November 11, 2004

Commencement June 2005

Master of Science thesis of Manish G. Bothara presented on November 11, 2004.

APPROVED:

_____

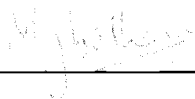Major Professor, representing Materials Science

_____

Coordinator of the Material Science Program

_____

Dean of the Graduate School

I understand that my thesis will become part of the permanent collection of Oregon State University libraries. My signature below authorizes release of my thesis to any reader upon request.

_____

Manish G. Bothara, Author

ACKNOWLEDGEMENTS

TABLE OF CONTENTS

TABLE OF CONTENTS (Continued)

LIST OF FIGURES

LIST OF FIGURES (Continued)

LIST OF FIGURES (Continued)

LIST OF FIGURES (Continued)

LIST OF TABLES

1. Introduction

Microelectromechanical Systems (MEMS) and Microtechnology based Electronic and Chemical Systems (MECS) have been in focus due to their technological potential and wide applications. Recently, there has been intense research activity in these areas [1]. In this study, an investigation into the bonding and embossing capabilities of bulk metallic glass forming alloy $Zr_{46.7}Ti_{8.3}Cu_{7.5}Ni_{10}Be_{27.5}$ (Vit4) has been made with the view of exploring its potential for use in fields such as MEMS and MECS. The main aim of this project was to determine the time, temperature and pressure parameters for bonding and embossing of Vit4. The size of the features that can be embossed on to the samples of Vit4 was also of particular interest.

1.1 Bulk Metallic Glasses

A crystalline solid has long range order which implies translational symmetry. In such a solid the atoms (or groups of atoms) are arranged in a pattern that repeats periodically in three dimensions throughout the grain. Solids that do not have a crystalline structure are termed as amorphous solids. Unlike metals which have a well defined crystal structure, the atoms of amorphous solids are distributed randomly if viewed on a long scale. What these solids do have is a short-range order which means that the atoms arrange themselves into small groups which are not repeated consistently throughout the bulk of the sample. This kind of structure is normally associated with liquids. When a liquid is cooled below its melting point, the atoms arrange themselves into a crystalline structure and the material

crystallizes into a solid. However, this is not always true. If the cooling rate is fast enough, the atoms will not have sufficient time to form a crystalline structure with long range order. If crystallization of the liquid is avoided below its melting point, the resulting liquid is known as a supercooled liquid. This supercooled liquid is characterized by a higher viscosity, which means a higher resistance to flow, than the liquid above the melting point. The viscosity increases as the temperature is decreased until the material is "frozen" on experimental time scale. Below this point, the material is termed to exist as a glass and the temperature corresponding to this point is the glass transition temperature, T_g. The ability of the material to be frozen into a glass is determined by the critical cooling rate, R_c. This is the slowest cooling rate required in order to avoid crystallization of the material. The thickness, t, of the metallic glass is inversely related to R_c.

$$(t \alpha 1 \big/ \sqrt{R_c}) \tag{1}$$

The first metallic glasses prepared in 1960 by Duwez using Au_3Si were only a few microns thick. They required cooling rates of 10^6 K/s and were prepared by splat quenching technique [2]. Two factors helped in improving R_c. First was designing of novel multi-component alloys having deep eutectics which provided materials with lower melting points. A schematic ternary phase diagram showing the ternary eutectic, E, is shown in Fig.1.
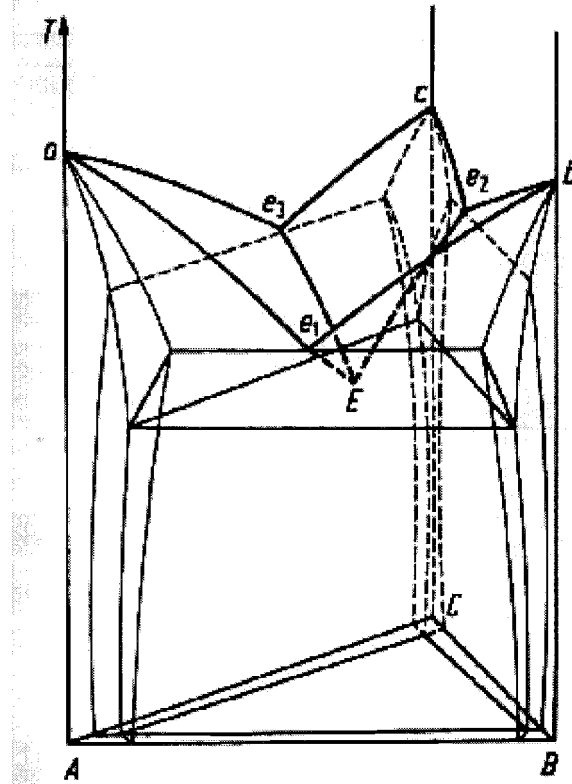
Figure 1: Schematic ternary phase diagram for an alloy system exhibiting a deep ternary eutectic, point E.

The second factor was the presence of different sized atoms in these multi-component alloys. This resulted in closer packing of the atoms and reduced mobility. So, as the material is cooled below the eutectic point the diffusivity falls sharply thus facilitating glass formation and reducing R_c. A Ni-Pd-P alloy having a critical cooling rate of approximately 10 K/s was the first bulk metallic glass (BMG). Bulk here means that the samples obtained had a thickness of few millimeters. This alloy was investigated by Drehman, Greer, Kui and Turnbull [3, 4]. Vitreloy 1^{TM}, $Zr_{41.2}Ti_{13.8}Cu_{12.5}Ni_{10}Be_{22.5}$, developed by A. Peker and W.L. Johnson at Caltech in 1992 has a critical cooling rate on the order of 1 K/s [5].

The reduction in critical cooling rates from 10^6 K/s to 1 K/s has increased the critical thickness from few micrometers to a few centimeters. $Zr_{46.7}Ti_{8.3}Cu_{7.5}Ni_{10}Be_{27.5}$, Vit4, which has been used in this study, has the same five elements as Vitreloy1^{TM} but varies in composition. The reason for choosing this alloy over Vitreloy1^{TM} is explained in chapter 2.1 below.

1.2 Microminiature Devices

Microelectromechanical Systems (MEMS) is the integration of mechanical and electrical components into a highly miniaturized device or an array of devices. The electrical elements like sensors, actuators, and electronics are fabricated using integrated circuit batch-processing techniques. The micromechanical devices are fabricated using compatible micromachining processes that selectively etch away parts of the silicon wafer or add new structural layers [6]. MEMS based devices are finding applications everywhere from the sensors in cars that trigger air bags to injectable drug delivery systems to environmental monitoring devices. Figure 2 shows a picture of an analog accelerometer in comparison to a USA stamp.

Figure 2: MEMS based analog accelerometer in comparison to a USA stamp [7].

For any application, MEMS devices are required to have a robust design with high reliability, increased efficiency, increased functioning and a long life. Technologists are busily ushering in a new age of miniaturization based on MEMS.

Microtechnology based Energy and Chemical Systems (MECS) are miniaturized fluidic devices with small and intricate features with dimensions on the order of few hundred microns. Figure 3 shows a picture of an intricate network of microchannels etched on a steel piece. Ongoing research aims to use these pieces for manufacture of a miniaturized heat pump to be fitted in body suits worn by soldiers and firefighters.
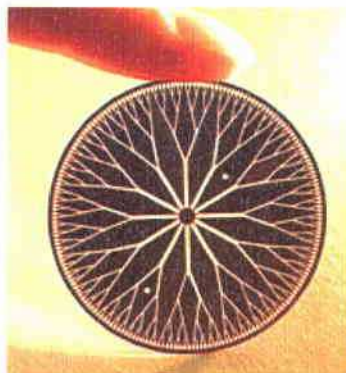
Figure 3: Microchannel array with fractal geometry designed by Dr. Deborah Pence, *et al.* at OSU.

MECS devices present opportunities for use in various applications. In the electronics industry power packs working on combustion principle instead of electrochemistry can improve the speed of electronic devices by a factor of ten [8]. Miniaturized refrigerators used for Joule-Thomson cooling of Electronic

Chips and Devices also have a similar effect [9]. Transportation and disposal of toxic byproducts released in various chemical processes can be eliminated by using miniaturized chemical reactors that would provide on-site neutralization of these toxic chemicals [10]. Miniaturized bioreactors could provide precisely regulated environments for small groups of cells to enhance their production of therapeutic drugs, or the detection of toxic compounds. Such biological applications could range from benchtop research to large scale production facilities.

1.3 Why use bulk metallic glass (BMG) for Microminiature devices?

A crystalline metal or alloy is replete with defects such as dislocations and grain boundaries. These defects make the structure weaker when compared to a grain boundary and dislocation free material. BMGs do not have a crystal structure and therefore are much stronger than their crystalline counterparts. For example, Vitreloy1™ has a tensile strength of 2 GPa while regular steels have tensile strengths ranging between 200-600 MPa. This property can be used to reduce weight of a micro device which is extremely desirable. Also with the invention of Zr based alloys, BMGs having excellent mechanical properties and high wear resistance are now available. MEMS devices often fail due to wear of micromechanical components. In addition, the MECS applications listed above require materials that are chemically inert and resistant to corrosion and have the ability to be made into extremely small components with micron level features.

The size and uniformity of the features is critical for effective operation of such a micro device.

The two most common ways of producing features on a substrate are injection molding and embossing. Micro-injection molding and hot embossing methods have been used to manufacture plastic based MEMS for use in medical industry [11,12]. These are depicted on a schematic Time-Temperature transformation diagram (TTT) in Fig. 4. Path 1 denotes the injection molding process that involves casting the molten material into a mold with desired features. Lack of crystal structure lends BMG with a very important property called net shape formability. It has been demonstrated that Vitreloy1^{TM} can be cast into molds with features on the level of few microns and even sub-micron features [13]. Path 2 in Fig. 4 represents the second approach which is to heat the material only up to a point where it can flow into the features of the die. This method is called as embossing and is used in this research. The viscosity of BMG is a strong function of temperature. This will be discussed below in chapter 2.2. Upon heating from room temperature, a drastic drop in the viscosity of BMG is observed close to its glass transition temperature. In this temperature range, the BMG is much more processible. It was hence estimated that it is possible to emboss micron level features into the BMG.
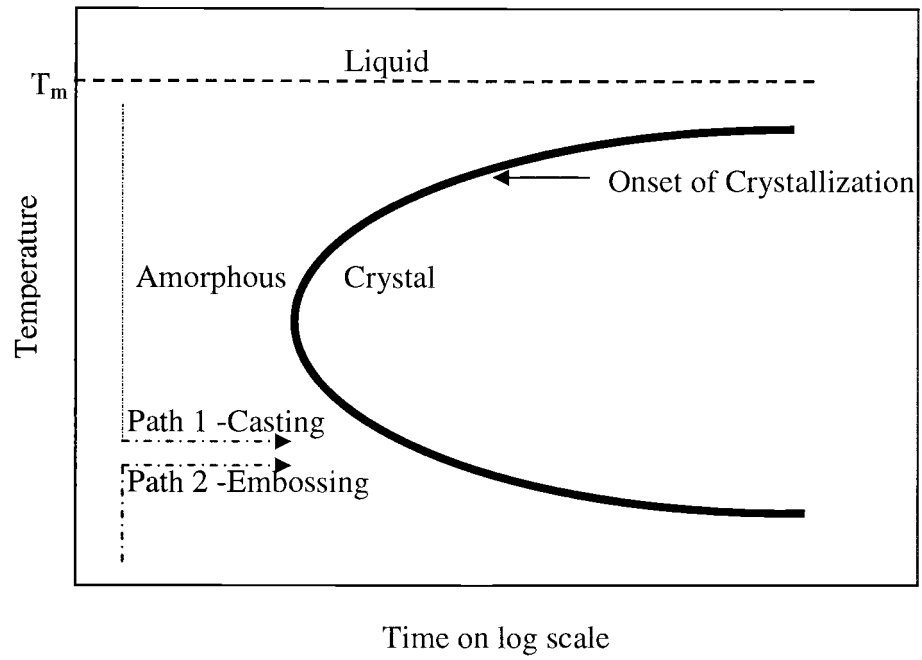
Figure 4: Two approaches to obtain micro-features on a material. T_m is the melting point.

2. Experimental Parameters

The reasons for selecting Vit4 over Vitreloy1^{TM} are discussed in chapter 2.1

below. In order to fabricate a micro device, for example a miniature heat

exchanger, two major processes need to be successfully carried out with the

BMG. First step is to emboss the features onto BMG substrates. This is achieved

by heating the substrate to a temperature where it becomes soft and by pressing a

die with desired features into the material. This results in a piece with embossed

features. The second step involves stacking and bonding of these substrates to

give an array of microchannels. A schematic diagram of these two steps and the

final device is shown in Fig. 5. This chapter introduces these two processes and

discusses the approach used to determine the experimental conditions.

Force application

Die

Substrate

Mold release

Embossed piece with

micro features

Stacking and Bonding

Array of microchannels
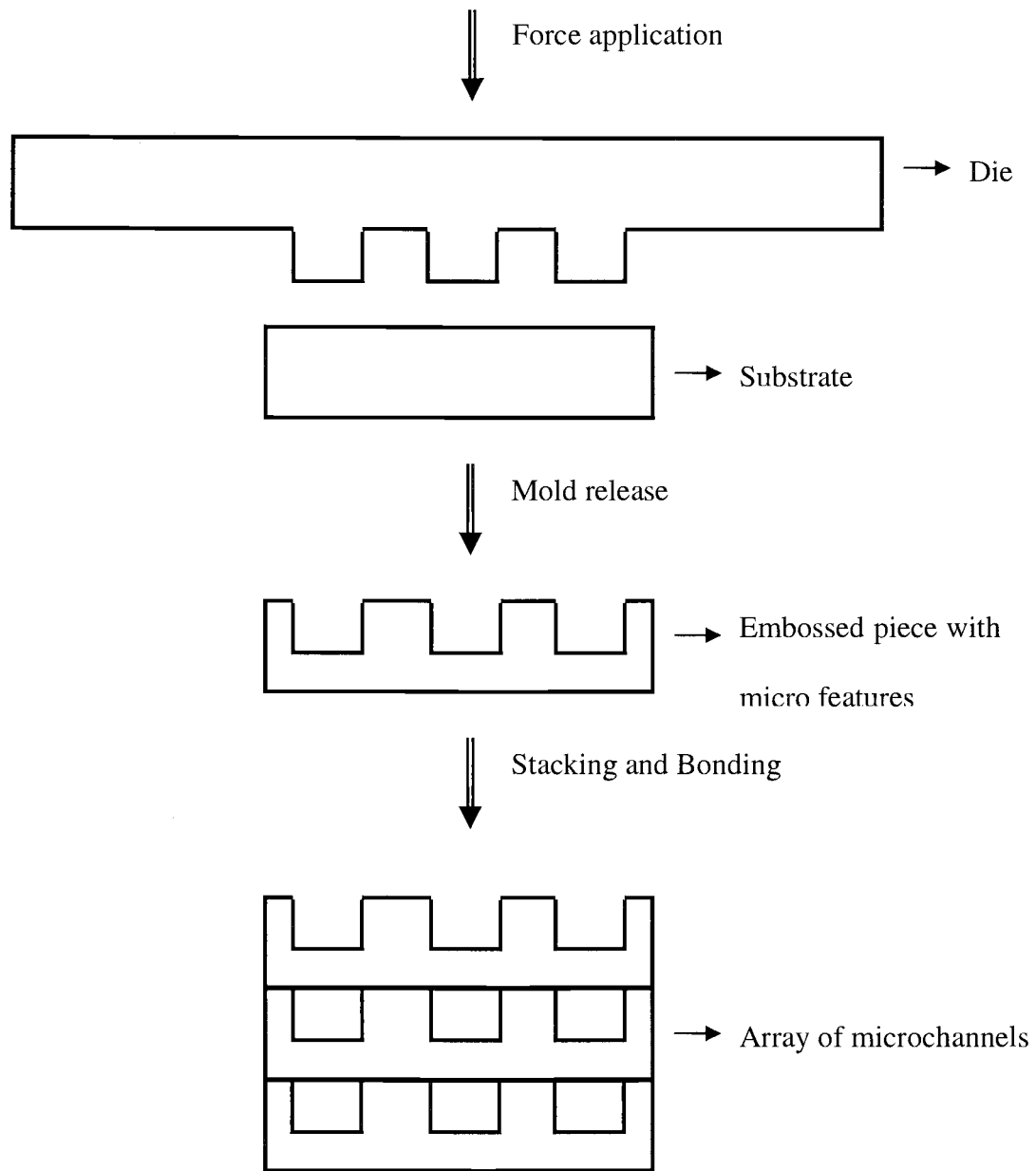
Figure 5: Schematic representation of the process involved in the manufacture of
a device consisting of an array of microchannels.

2.1 Comparison of Vitreloy1™ and Vit4

The reason for choosing Vit4 ahead of Vitreloy1™ for diffusion bonding and embossing is briefly explained in this section. Differential Scanning Calorimeter (DSC) is the most widely used thermoanalytical technique that provides fundamentally sound measurement of heat flow as a function of time and temperature.

2.1.1 Principle of DSC

It consists of two isolated pans, sample and reference. Both have individual heaters and sensors to measure the power that is supplied in order to keep the sample and reference pans at the same temperature during heating, cooling or isothermal cycles. Typical DSC scan obtained by continuously heating a BMG specimen at a steady heating rate is shown in Fig. 6. Here, it depicts the phase transitions that occurred during the first heating cycle. Initial small endothermic peak corresponds to the glass transition, T_g, and provides the proof for initial glassy state of the specimen. Upon further heating crystallization occurs exothermally and finally the sample melts. The melting peak is endothermic and is not shown here.
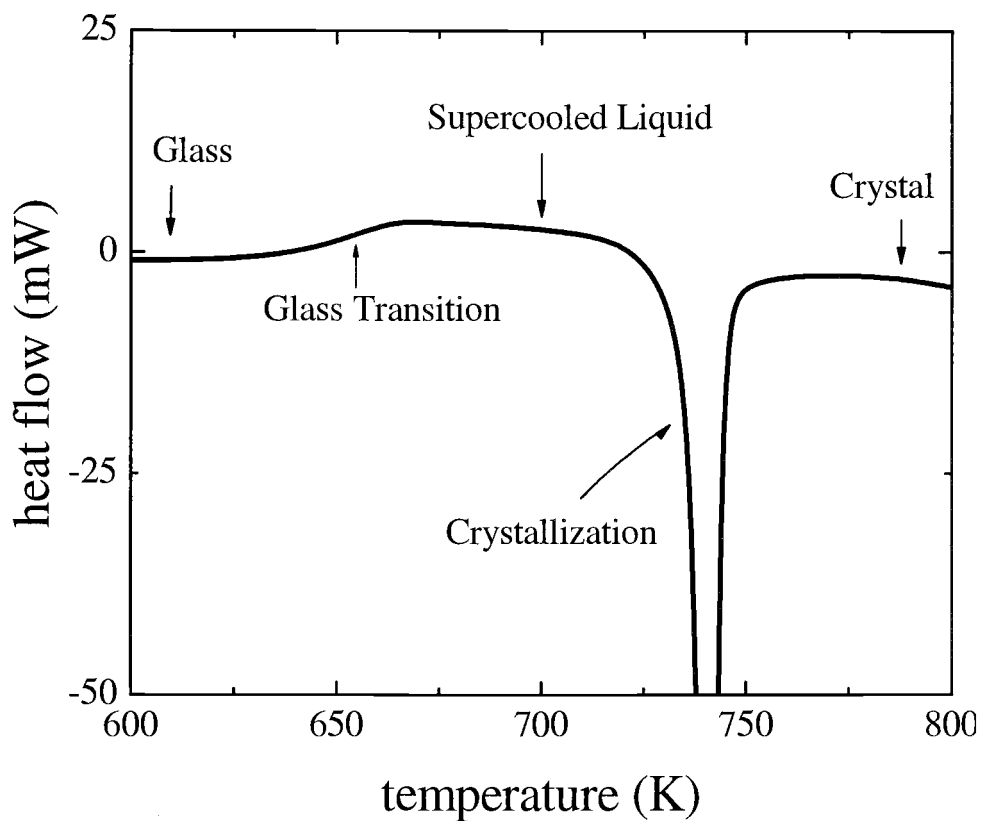
Figure 6: A typical DSC scan of BMG sample.

2.1.2 Crystallization in Vitreloy1™ and Vit4

A comparison of DSC scans of Vitreloy1™ and Vit4, which are shown in Fig. 7

(a) and (b), reveals that although these two alloys have the same component

elements, crystallization in Vitreloy1™ proceeds in a different manner than Vit4.
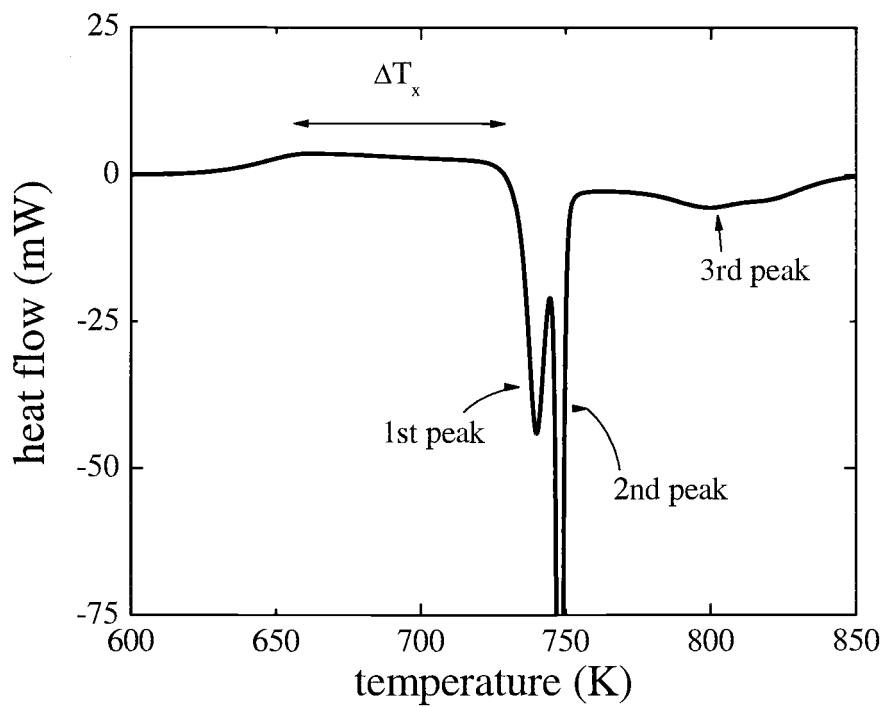
(a)
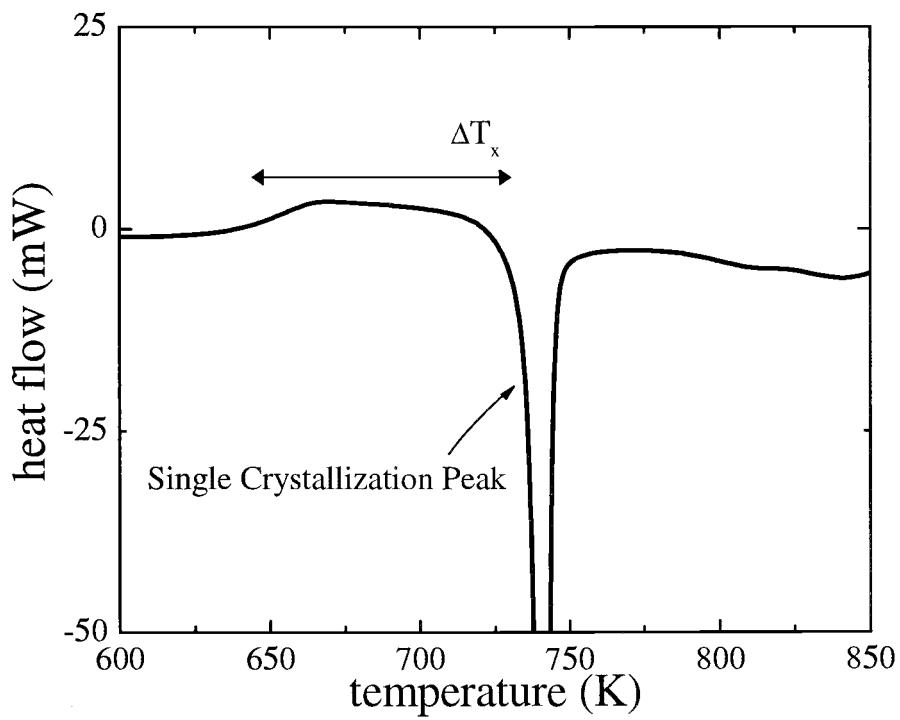
(b)

Figure 7: Typical DSC scans for (a) Vitreloy1^{TM}, (b) Vit4

Vit4 exhibits a single peak suggesting that crystallization is a single event while in Vitreloy1[TM] there are three crystallization peaks. Busch *et al.* have explained this as a phase separation region. Vitreloy1[TM] decomposes into two phases, first phase undergoes nanocrystallization and the second phase is still an amorphous matrix. The nanocrystals remain embedded in the first amorphous phase and the second amorphous phase acts as the matrix. This decomposition leads to a substantial increase in the viscosity of Vitreloy1[TM]. Hence, it was concluded that it would be difficult to emboss and bond the decomposed Vitreloy1[TM]. The nanocrystals act as nucleation sites for the bulk crystals and this leads to the crystallization of the suspended amorphous phase in the decomposed Vitreloy1[TM]. The decomposition into two phases accompanied by the nanocrystallization followed by the crystallization of the first amorphous phase are responsible for the first two peaks in the DSC scan for Vitreloy1[TM]. The remaining amorphous matrix crystallizes last and corresponds to the third peak. This multistage crystallization for Vitreloy1[TM] is schematically shown in Fig. 8.

(a)   (b)   (c)   (d)
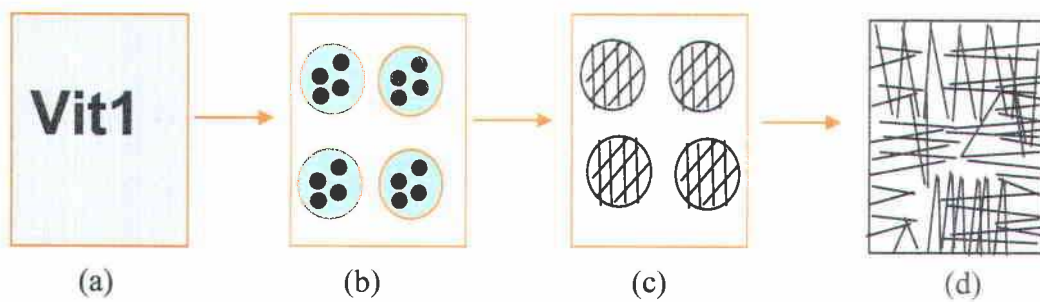
Figure 8: Schematic representation of the three step crystallization process of
a) pure Vit1, b) Phase separated Vit1 with nanocrystals embedded in the
first amorphous phase, c) Partially crystallized Vit1 with nanocrystals
causing the crystallization of the first amorphous phase, and
d) Complete crystallization of Vit1.

If heated at a constant rate through its glass transition temperature Vit4 does not phase separate and this is evident from the single crystallization peak. But when annealed, Vit4 also undergoes phase separation like Vitreloy1[TM] [14]. The DSC scan of an annealed Vit4 sample consists of two crystallization peaks each corresponding to one of the amorphous phases. This implies that phase separation is not accompanied by nanocrystallization. The two step crystallization process along with the DSC scan is shown below schematically in Fig. 9. The Vit4 sample in Fig. 9(a), separates into two amorphous phases A1 and A2, as shown in Fig.9(b), with slightly different compositions. First A1 crystallizes, Fig. 9(c) and this corresponds to the first peak in the DSC shown in Fig. 9(e). Now the remaining phase, A2, crystallizes leading to a completely crystallized sample as in Fig. 9(d). The crystallization of the second amorphous phase A2 is responsible for the second peak in the DSC signal.

(a)   (b)   (c)   (d)
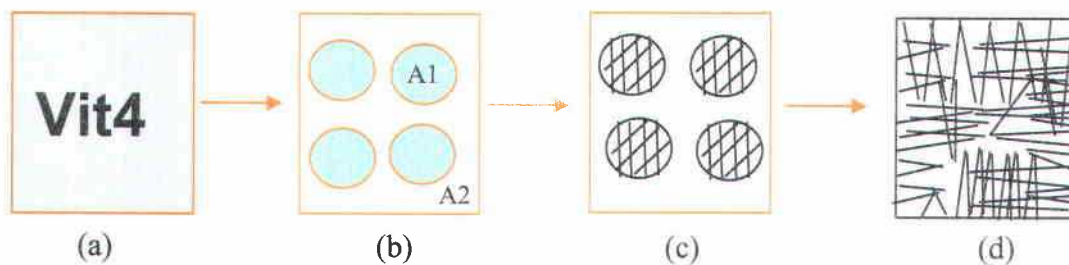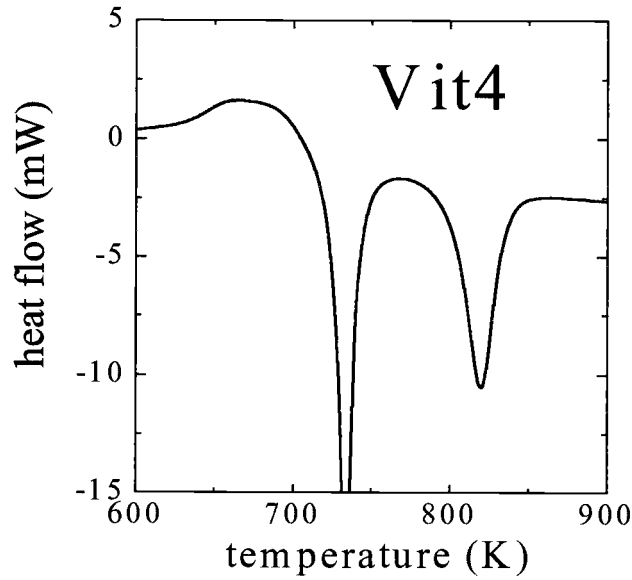
(e)

Figure 9: Schematic representation of the two step crystallization process of a)
pure Vit4 sample, which on annealing at 625 K for 1 hr,
(b) decomposes into two amorphous phases with different
compositions, c) Phase A1 undergoes crystallization to give partially
crystallized Vit4, d) Second phase crystallizes leading to complete
crystallization of Vit4, (e) DSC scan of an annealed Vit4 sample
showing two crystallization peaks.

Phase separation is undesirable as it is believed to be accompanied by an increase

in viscosity. This reduces the available annealing times and temperatures. But Fig.

7 shows that Vit4 has a larger supercooled liquid region, ΔT_x, than Vitreloy1^{TM}.

Therefore the times before crystallization occurs are much bigger in Vit4. Hence,

the time-temperature window within which diffusion bonding and embossing

experiments can be performed are substantially wider in Vit4 than in Vitreloy1^{TM}.

This is attributed to kinetics above but close to T_g which are more sluggish in Vit4

than in Vitreloy1^{TM} [15].

2.2 Embossing

Embossing is the process of creating three-dimensional parts, lettering, and other surface definition onto materials. This is achieved through the use of forms and dies, which are forced into the surface of the material by extreme pressure or raising the temperature of the material or both. When removed, the patterns on the forms and dies are indelibly stamped into the material. Embossing forms microstructures in thermoplastic polymers by replicating the features on a die into a thermally softened material. This technique is a cost-effective high-throughput process, and is well suited for manufacturing. (xing, wang, han). The manufacturing of compact disks (CDs) based on imprinting in polycarbonate with a Ni master is a typical example of large-volume commercial application of embossing [16]. Lately this technique has been looked at as a method for making nanometer-size (<50nm) structures on semiconductors, metals, and other materials commonly used in microelectronic circuitry. Embossing, for example, has also been used by Chou *et al.* [17] to generate features in Si with lateral dimensions as small as ~25 nm. This technique was also examined as a potential method for replicating binary optical components with feature size smaller than 100 nm [18,19]. Three main parameters in all these experiments are time, temperature and pressure. The material needs to be heated to a temperature where it can readily take the shape of the die that is being pressed into it. In the case of BMG like Vit4, the force required is a strong function of the viscosity of the material at the embossing temperature.

The viscosity, η, of Vit4 as a function of temperature, T, has been measured by E.

Bakke, R. Busch and W. L. Johnson using parallel plate rheometry [20]. They

found that the equilibrium viscosity data can be fitted well with the Vogel-

Fulcher-Tammann (VFT) relation [21]

$$\eta = \eta_0 * \exp[DT_0 / (T-T_0)] \tag{2}$$

in which $D = 22.7$ is the fragility parameter and $T_0 = 372$ K is the VFT

temperature. D is a measure of the fragility of a glass. D for silicate glasses, which

are very good glass formers, is around 100 while for poor glass formers like

rubber and o-Terphenyl is around 2. Amorphous materials with a higher value of

D are called strong glasses while those with lower values of D are called fragile

glasses. Hence D is an indicator of glass formability of a material. It should be

noted that the terms strong and fragile glasses do not mean that the material is

mechanically strong or fragile. T_0 is the temperature at which the barriers with

respect to flow go to infinity. The viscosity of all the liquids at infinite

temperature converges to $\eta_0 = 10^{-4}$ Pa.s. Thus, as shown in Fig. 10 below, the

viscosity decreases sharply with increasing temperature. Therefore, Vit4 becomes

soft as embossing temperature increases, and hence the required force and the

embossing time decreases.
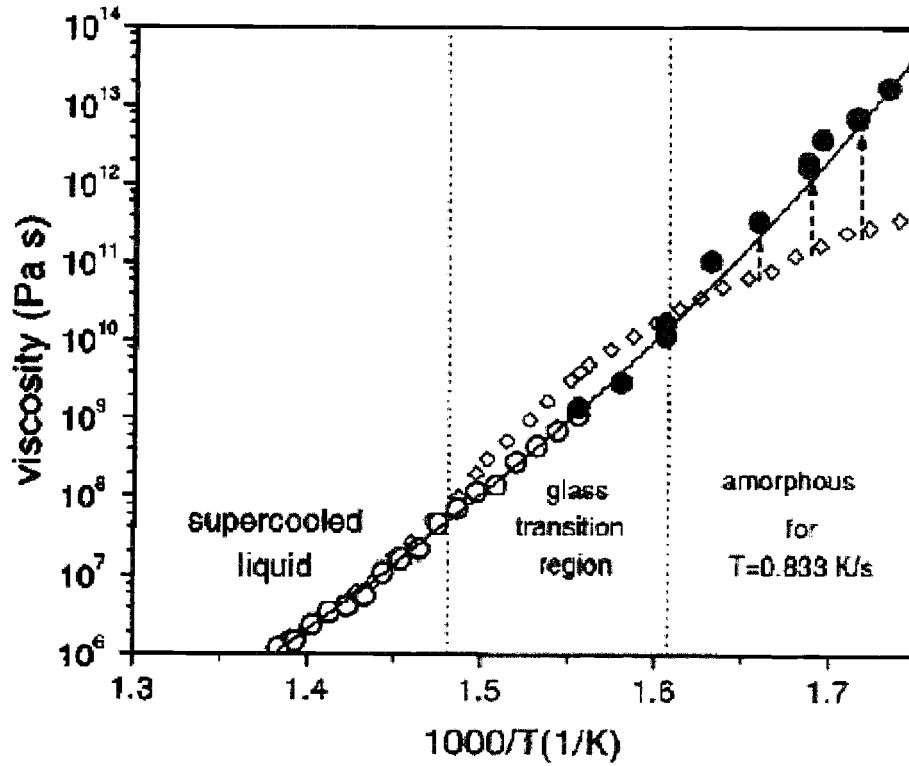
Figure 10: Viscosity as a function of inverse temperature measured for Vit4 close to its glass transition. [21]

For a parallel plate experiment the correlation between the viscosity of a sample and its rate of change of height at a certain temperature is given by the Stefan equation [22, 23].

$$\eta = \frac{-2Fh^3}{3\pi a^4 \left(\dfrac{\Delta h}{\Delta t}\right)} \tag{3}$$

Here, F is the load on the sample, 'a' is the radius of the plate and 'h' is the initial height. The viscosity of the sample at a given temperature, T, is known from Fig. 10. This relation was used to estimate the embossing time Δt for a given reduction in height Δh, load F and initial sample dimensions of h and a. To obtain the dependence of embossing time Δt on viscosity, the values of F, h, a and Δh were

fixed as shown in Table I.

Table I: Variables in Eq. (3) that had fixed values for the calculation
of experimental parameters.

Force on sample, F = 890 N
Initial Sample Height, h = 1mm
Reduction in Height, Δh = 100 μm
Radius of Plate, a = 4.674 mm

So, for example, for temperature, T = 640 K Eq. (2) yields a viscosity value of η = 1.93*10^9 Pa.s. Using the above values in Eq. (3) gives, Δt = 488 s.

As the temperature and deformation are varied, a set of values for Δt are obtained as presented in Table II. As the temperature increases viscosity falls drastically and the time required for a certain deformation decreases.

Table II: Embossing times Δt for Δh varying from 500 nm to 500 μm.

Temp	Viscosity	Δt (at different Δh)						
K	Pa.s	500 nm	1 μm	5 μm	10 μm	50 μm	100 μm	500 μm
600	4.86E+11	615	1229	6145	12290	61451	122903	614514
610	1.03E+11	130	259	1296	2593	12963	25925	129627
620	2.45E+10	31	62	310	620	3100	6200	31000
630	6.56E+09	8	17	83	166	828	1657	8283
640	1.93E+09	2	5	24	49	244	488	2442
650	6.22E+08	0.79	2	8	16	79	157	786
660	2.17E+08	0.27	0.55	3	5	27	55	274
670	8.10E+07	0.10	0.20	1	2	10	20	102
680	3.23E+07	0.04	0.08	0.41	0.82	4	8	41
690	1.36E+07	0.02	0.03	0.17	0.34	2	3	17
700	6.07E+06	0.01	0.02	0.08	0.15	0.77	1.53	8

Thus the time required for a desired deformation at a certain temperature was established. But whether Vit4 crystallized within this time is given by the Time Temperature Transformation (TTT) diagram.

2.2.1 Time Temperature Transformation (TTT) diagram

The Time Temperature Transformation diagram for Vit4 is obtained through

isothermal experiments at various temperatures, which terminate with crystallization of the material. The temperature is plotted on the vertical axis and the time is plotted on the horizontal axis on a logarithmic scale. In such TTT diagrams the time required for crystallization as a function of temperature is represented by various curves, such as the onset (1%), intermediate (~50%) and end (99%) time of crystallization, are represented by such TTT diagrams. As described in section 1.2, a glass is formed by avoiding crystallization of the material below its melting point. The driving force for crystallization increases as the material is cooled more and more below its melting point. But the diffusivity of the components in the alloy also decreases exponentially as the temperature is decreased. The slowing down of the kinetics (reduced diffusivity) below the melting point and the increased driving force for crystallization are opposing forces. Hence, the characteristic "C" shape of the TTT diagram. As the material is cooled below its melting point the time taken for initiation of crystallization decreases. The increase in the driving force for crystallization controls the crystallization process. This trend continues till the nose of the TTT diagram is reached. The nose corresponds to minimum amount of time required to initiate crystallization at any undercooling. Below the nose sluggish kinetics of the system takes over and determines the crystallization onset. The crystallization proceeds in different manner in various alloys.

The TTT diagram for Vit4 was traced for temperatures close to its glass transition using a Differential Scanning Calorimetry (DSC). The onset of crystallization time for Vit4 close to its glass transition are plotted in Fig. 11 and compared with

data previously measured by Busch and Johnson [24].
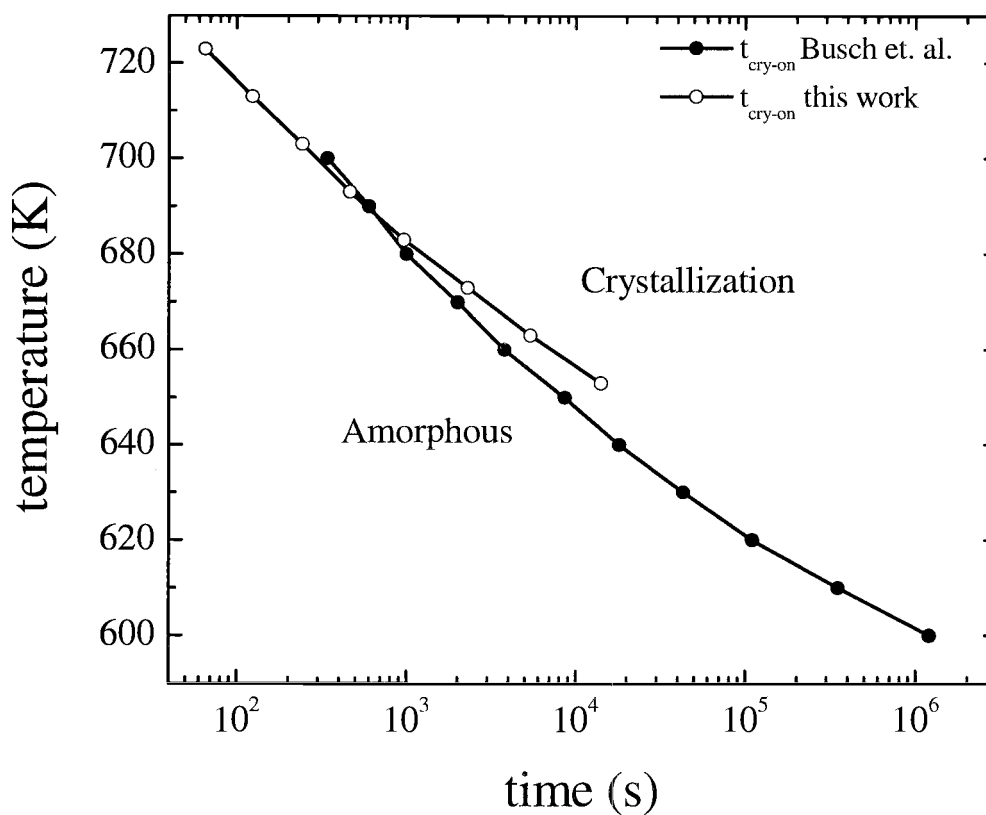
Figure 11: Time temperature transformation diagram for Vit4 measured by Busch
et al. [24] and measured in this research using the DSC.

In order to compare t_{cry-on} with Δt, the data in Table II was plotted on the TTT

diagram for Vit4 which is reported in Fig. 12.
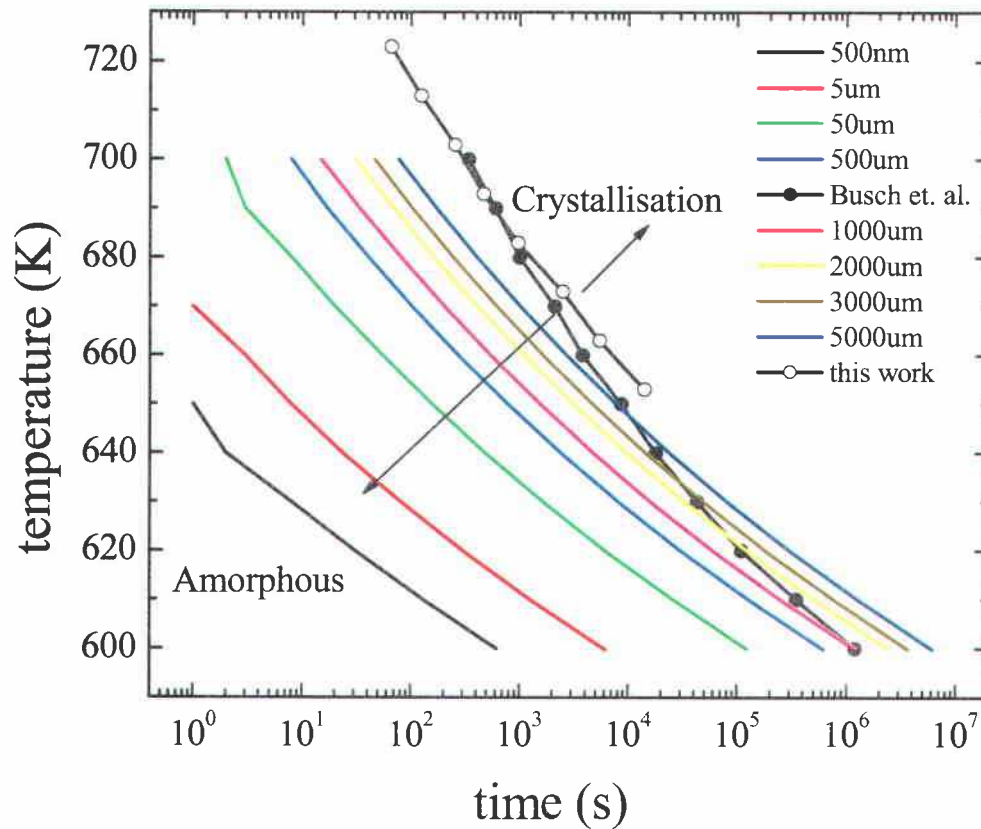
Figure 82: Uniform-Deformation curves for Δh varying from 500 nm to 5000 μm.

It is proven in Table II that for a parallel plate geometry (where Stefan's relation is valid) the time required for embossing decreases strongly with increasing temperature and decreasing deformation. For example, one would require 786 s to deform the sample by 500 μm at 650 K while it takes only 102 s at 670 K. Similarly it only takes 157 s to deform 100 μm at 650 K. At the same time it takes 8600 s for Vit4 to crystallize at 650 K. Hence, a time-temperature window was established for conducting embossing experiments. According to Fig. 12 it is possible to deform the material by 1000 μm without crystallization using a 890 N force.

2.3 Diffusion Bonding

2.3.1 Introduction to Diffusion Bonding

Welding processes can be classified into fusion welding and pressure welding. When two pieces are permanently joined together due to the formation of interatomic bonds the process is termed as welding. Fusion welding is the joint formed due to local or general heating of the workpieces above their melting point. Pressure welding occurs due to plastic deformation at the interface of the substrates. The deformation leaves the surfaces rough hence they seize each other. Diffusion bonding of materials in solid state is a process for making a monolithic joint through the formation of bonds at atomic level, as a result of closure of the mating surfaces due to local plastic deformation at elevated temperature which aids interdiffusion at the surface layers of the materials being joined. The success or failure of the process is determined by three variables which need a constant watch and careful adjustment. These are bonding temperature, the bonding pressure (or pressing load), and the holding time (duration of pressure). These bonding variables vary according to the kind of materials to be joined, surface finish, and the expected service conditions.

2.3.2 Mating Surfaces

To achieve interatomic bonding between two surfaces, the workpieces must be brought to within the atomic spacing. This would require ideally smooth surfaces,

which are flat down to Angstrom level. Real surfaces are never ideally smooth or clean. Even an extremely carefully polished surface will show microscopic asperities with a height of several hundreds or even thousands of molecular layers. Also the surface of any solid has atoms with unsatisfied bonds at its surface which are called hanging bonds. Hence, the surface of any solid holds atoms from the surrounding medium, above all oxygen atoms, which form strong chemical bonds with the surface atoms. As a result of this uneven surface geometry, chemical conditions, and physical state when two pieces are brought together, they will only come in contact at asperities.

2.3.3 Mechanisms of Bond Formation in Diffusion Bonding

Several hypotheses have been advanced to explain how a bond is formed in solid state. The *Film hypothesis* [25] proposed by S. B. Ainbinder *et al.* states that when metal and alloys with clean surfaces are brought together within the range of interatomic forces they have an tendency to cease.

The *recrystallization hypothesis* [25] puts emphasis on recrystallization as the principal factor in bond formation. By this hypothesis, deformation and the accompanying strain hardening, coupled with exposure to relatively high temperatures at the interface, cause the atoms in the lattices of the materials being joined to move to other sites so that there appear, at their boundaries, grains common to both pieces with the result that a bond is formed.

According to the *energy hypothesis* [25], for a diffusion bond to form the atoms of

metals being joined should be raised to what may be called the energy threshold of seizure or adhesion. At this threshold, the orientation of atomic bonds is no longer a factor. Metallic bonds come into being between the atoms at the surfaces, and the interface between the two pieces disappears.

J. Fredel, E. I. Astrov, *et al.* suggest that the joint plastic deformation causes dislocation to move to the surface. In doing so, they break up the oxide films present and produce steps each an interatomic distance high. This is termed as *dislocation hypothesis* [25], in which the emergence of dislocations at the contact surface reduces resistance to plastic deformation and aids in joining the metals. In the *electron hypothesis* [26] advanced by G. V. Somsonov *et al.*, the surface seizure results in the formation of stable electron configurations involving the atoms of the metal in contact.

In accord with the *diffusion hypothesis* [27-31], the formation of a sound bond between the surfaces in contact depends on the interdiffusion of atoms into the bulk of the specimens. The surface atoms of a metal have free, unfilled bonds (vacancies) which capture any atom moving within the range of interatomic forces. In solids, a substantial amount of energy has to be put in, and elaborate techniques have to be used in order to bring the atoms closer together within joining distance.

Despite the simplicity of the process, pressure welding involves a sequence of stages or steps, the surfaces to be joined are first brought in contact; the surface oxide and adsorbed films are then broken up; the surface layers are activated as a result of deformation; volumetric diffusion processes take place, recrystallization

follows, etc. These stages, undoubtedly overlapping in actual practice, testify to the complexity of pressure welding, because of which the mechanism of the process cannot, at times, be explained from a single point of view. Yet most investigators agree that pressure welds are produced as a result of the metallic bonds that form between the metals being joined.

The weight of material A going across unit area of material B, in unit time under unit concentration gradient is defined as the diffusivity of the material A in B, D_{AB}. It is typically known for diffusion-controlled process that the distance traveled, x, by an atom of material A while diffusing in B for time t, varies in proportion to the square root of t and is given approximately by the relation

$$x \sim \sqrt{D_{AB} * t} \tag{4}$$

2.3.4 Multi-component Alloys and Glass Formability

BMG are multi-component alloy systems with huge difference in the atomic size of the largest and the smallest component. Mixing atomic species with large size mismatch results in a crystalline alloy with chemical disorder. This chemical disorder is associated with local atomic strains arising from atomic size difference as well as differ ence in valence electron configuration of constituent species. Also, going from one element to five-element system, the probability of forming new crystal structures and a chance of getting periodically ordered structure progressively diminishes [32]. This leads to what is called as topological frustration [32] of the crystal formation and improves the glass forming ability of the alloy.

2.3.5 Atomic Size and Diffusivity

In general the diffusivity of the various atoms in an alloy varies inversely to their atomic size. The difference in the diffusivity becomes significant at lower temperatures. It is thus important to compare the diffusivities of each of the species in the alloy. Table III lists the elements of Vit4 with their atomic sizes.

Table III: Atomic size of components of Vit4.

Element	Atomic Radii (pm)
Zr	216
Ti	176
Ni	162
Cu	157
Be	112

Diffusivity, D, of various elements can be compared by plotting D against reciprocal temperature. In Fig. 13 data for Ni diffusion [33] are compared with data for Al [34], Be [15], B [35], Fe [35] and Co [35, 36] diffusion.
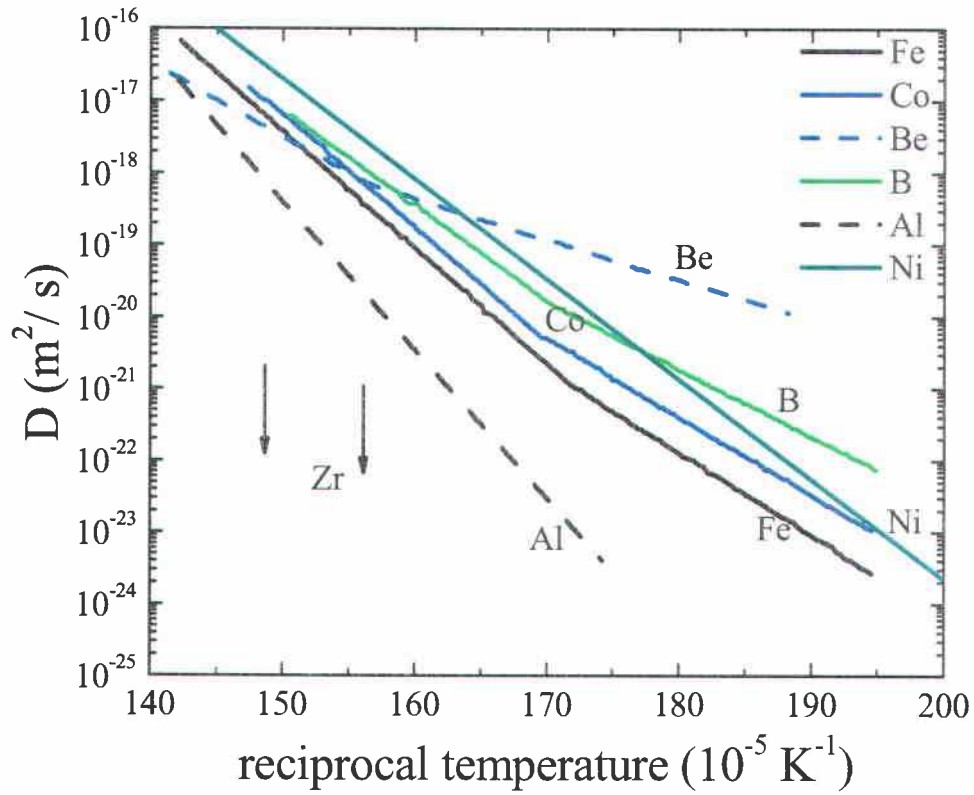
Figure 13: Diffusivities of various elements in Vit4.

Figure 13 illustrates that as temperature decreases (from left to right in this case), the diffusivities of various elements differ significantly from each other. For temperatures below 630 K, the Be atoms diffuse fastest through Vit4, while Zr being the largest atom is the slowest. Ni is slower than Be but has a higher diffusivity than Zr. This difference in diffusivity between different sized species becomes more pronounced with decreasing temperature. Diffusivity of Ni in Vit4 has been shown by Knorr *et al.* to follow the relation

$$D = \left(4.32^{+9.76}_{-2.99}\right) \times 10^3 \left(-\frac{(266 \pm 6)kJmol^{-1}}{RT}\right) m^2 s^{-1} \qquad (5)$$

With this information, the time required for diffusion of Ni for a constant

diffusion length can be plotted as a function of temperature. Table IV shows the

calculation of diffusion time, t, for Ni to diffuse 100 nm at 600 K.

Table IV: Calculation of diffusion time, t, using Eq. 4 and Eq. 5.

Sample calculation
T = 600 K
x = 100 nm
$D = 3 \times 10^{-20} \, m^2/s$
$t = x^2 / D = 3.33 \times 10^5 \, s = 92.5 \, hrs$

Results of conducting the above calculations for various diffusion lengths from 50

nm to 1 μm are charted in Table V below.

Table V: Diffusion times for various diffusion lengths from
50 nm to 1 μm at different temperatures.

Temp	D	time for different x (diffusion lengths)			
K	m^2/s	50nm	100nm	500nm	1μm
600	3.00E-20	8.33E+04	3.33E+05	6.75E+06	3.01E+07
620	1.68E-19	1.49E+04	5.97E+04	1.21E+06	5.38E+06
640	8.41E-19	2.97E+03	1.19E+04	2.41E+05	1.07E+06
660	3.82E-18	6.54E+02	2.61E+03	5.29E+04	2.36E+05
680	1.59E-17	1.57E+02	6.28E+02	1.27E+04	5.67E+04
700	6.10E-17	4.10E+01	1.64E+02	3.32E+03	1.48E+04

Figure 14 gives a plot of the diffusion time as a function of temperature for various diffusion lengths from 50 nm to 500 nm. The onset of crystallization curve for Vit4 is also given for comparison.
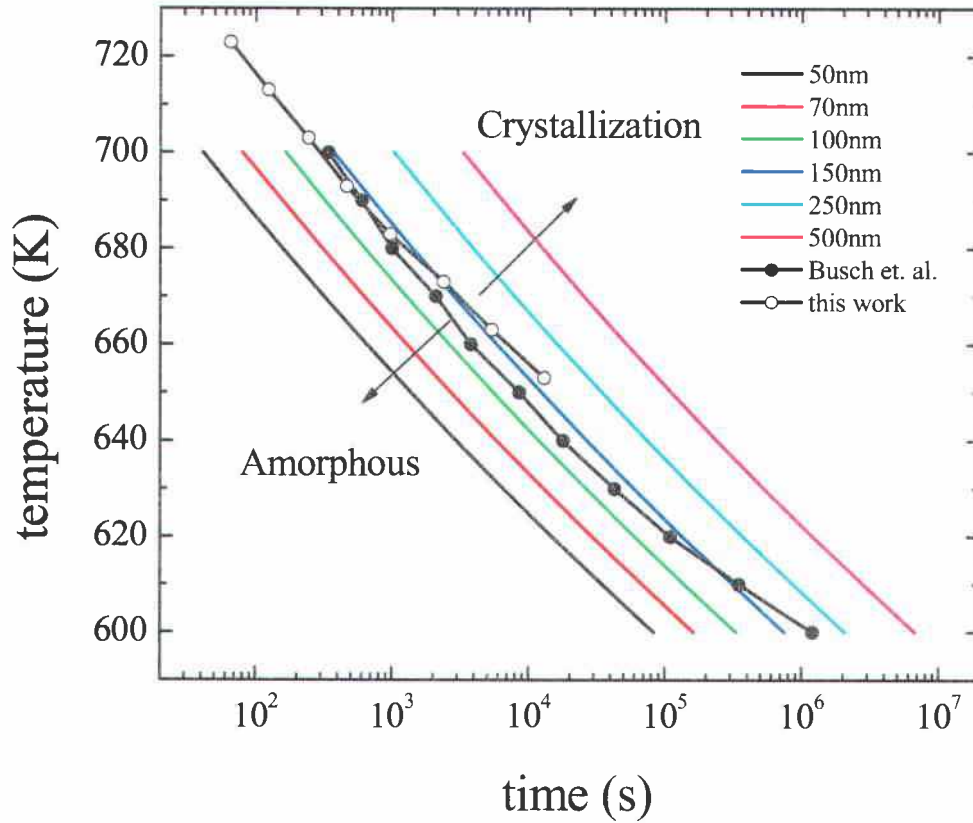
Figure 14: Uniform diffusion length curves. The TTT measured in this study is also shown for comparison.

In addition to being chemically similar, Al has a larger diffusivity than Zr in Vit4. Also, Al (r = 182 pm) and Ti (r = 176 pm) have similar atomic radii. Thus, Al diffusion mimics the diffusion of Ti and gives an upper limit for Zr diffusion [33] in Vit4. Figure 15 is obtained on plotting diffusion times, t, calculated using Eq. (4) for different Al diffusion lengths.
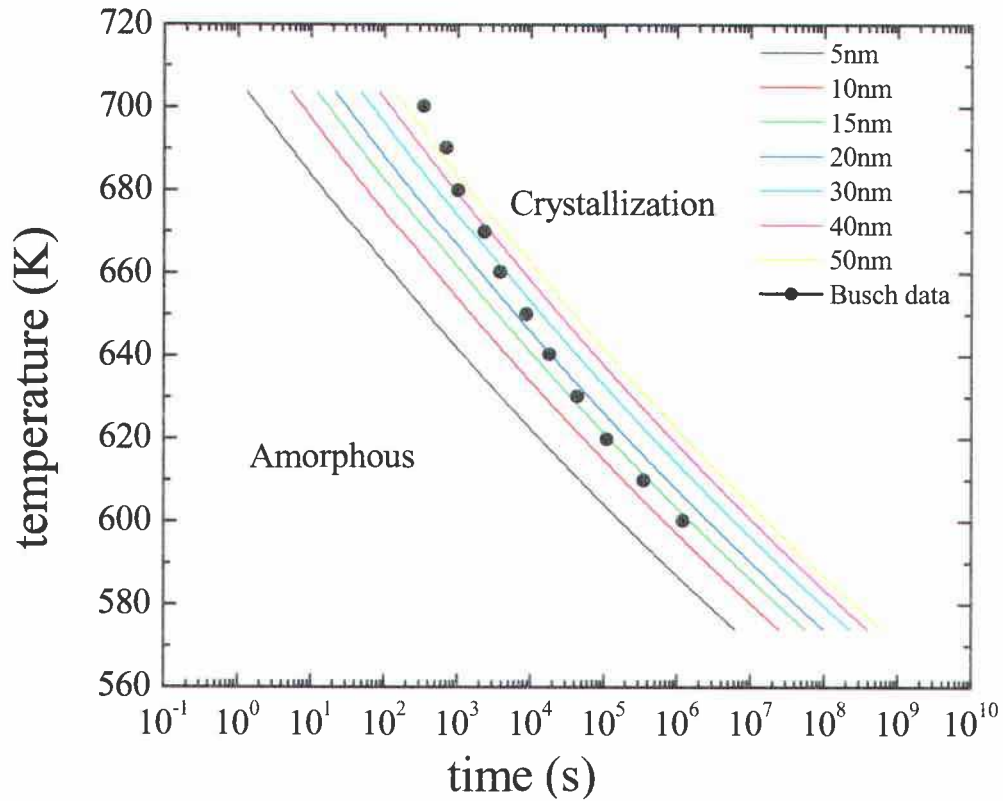
Figure 15: Uniform diffusion length curves for Al, which mimics the diffusion of Ti in Vit4 as Al and Ti have similar atomic radii. The TTT measured by Busch *et al.* [24] is given for comparison.

From Fig. 14 and Fig. 15 it can be established that a maximum diffusion length of around 150 nm for Ni and around 50 nm for Ti (approximated by Al diffusion) can be obtained before Vit4 crystallizes. Zr_2Cu is the primary crystalline phase that is formed on crystallizing Vit4. Ti, having a large atomic size, can replace Zr to a certain extent in the crystal structure of Zr_2Cu. Thus, it is likely to form Ti-enriched phases like $(ZrTi)_2(CuNi)$. Also note that Cu and Ni having similar atomic radii can substitute each other. Thus, it was likely that concentration redistribution of Ti, which is the second largest component with respect to the atomic size, will lead to crystallization.

L. Shadospeaker, M. Shah and R. Busch have suggested similar trends for $Zr_{57}Cu_{15.4}Ni_{12.6}Al_{10}Nb_5$ [37], a BMG forming alloy, in which Al and Nb concentrations have to undergo severe redistribution in order to form the crystalline phases. This implied that if the big atoms, like Zr and Ti in Vit4, were not allowed to diffuse then crystallization can be avoided. Thus, it was investigated whether the diffusion of medium sized atoms, like Cu and Ni, is sufficient for forming a bond between the two surfaces without crystallizing the alloy.

3. Experimental Procedure

3.1 Sample preparation

An amorphous alloy rod with nominal composition of Vit4 was supplied by Liquidmetal Technologies Inc., the leading manufacturer of products made from amorphous alloys. It was prepared by melting a mixture of the elements of purity ranging from 99.5% to 99.9% by induction melting and subsequent water quenching in a 12.5 mm diameter steel tube. After quenching, the steel tube with the sample in it is passed through a roller. Coming out of the roller the tube gets flattened along the vertical axis and elongated in the horizontal axis. The steel tube is stripped out and an amorphous rod of Vit4 with elliptical cross-section is obtained.

The cross-sectional face of the rod was polished first using standard polishing procedures which ended with 0.05 μm polishing wheel. Once a face was polished, a 1 mm thick sample was cut from that face using a precision ISOMET^{TM} 5000 diamond saw. Using this method several 1 mm thick samples of Vit4 were prepared with one polished face.

3.2 Profiling of samples

As mentioned in section 2.3.1, it is important to know the surface roughness of the sample. A Veeco^{TM} Dektak^{TM}8 stylus surface profiler was used to measure the surface roughness of all the samples. The arithmetic average deviation from the

mean line is called arithmetic average roughness, R_a and is the most used international roughness parameter. Total waviness, W_t, measures the difference between maximum peak height and maximum valley depth from the mean line. The average roughness, R_a, and waviness, W_t, values were averaged over six different measurements on each sample. Three measurements were taken along the length while three were taken perpendicular to it. One such measurement demonstrating the roughness and waviness profiles is shown in Fig. 16. The waviness for this sample, denoted by the blue line, is $W_t = 4.09$ µm profile while the roughness, denoted by the red line, is $R_a = 20$ nm.
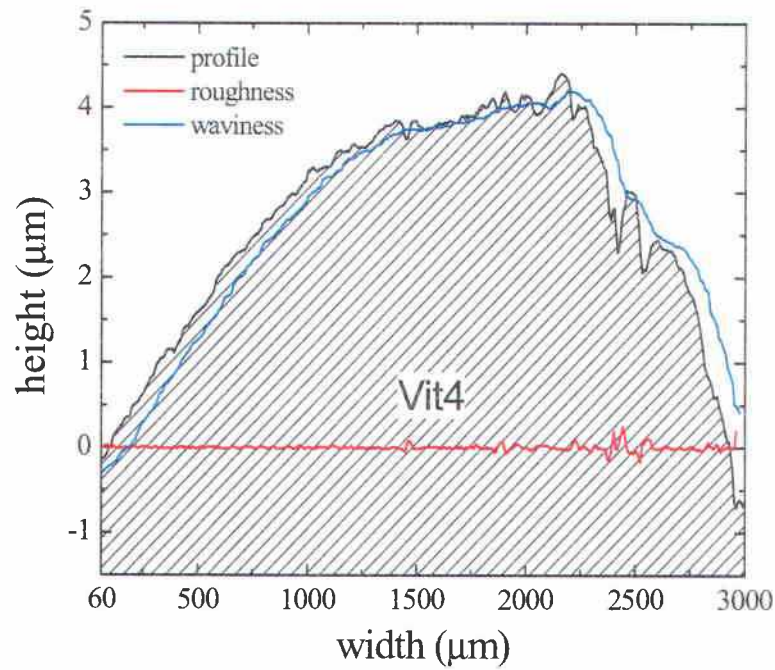
Figure 16: Roughness profile (red line) and Waviness profile (blue curve) are shown. For this sample $R_a = 20$ nm and $W_t = 4.09$ µm.

The average values of R_a and W_t for five samples are listed in Table VI.

Table VI: Average values of R_a and W_t for five samples.

Sample No.	R_a (nm)	W_t (µm)
1	5.2	11.3
2	4.1	13.45
3	5.7	14.4
4	4.0	14.16
5	4.0	23.12
Average	4.6	15.29

The temperatures for all the bonding and embossing experiments were above 620 K. According to the Stefan equation, Eq. (3), the time it takes for a flow depth of 20 µm under a load of 890 N at 625 K is about 650 s. Hence, it can be assumed that the asperities would be flattened after 650 s and intimate contact will be established between the mating surfaces.

For bonding experiments two samples prepared as described above were stacked with their polished surfaces in contact. A single sample was used for each embossing run.

3.3 High Temperature High Vacuum Hydraulic Press

Diffusion bonding is carried out in suitably designed units that are fairly simple in their arrangement. A Pressmaster vacuum hot press model HP30-4560 from Thermal Technologies Inc. with Eurotherm 2404 temperature control unit and type K thermocouples was used in this study. The force on the press was

measured with an OMEGA high performance strain gauge indicator. The main

components of the press are as depicted in Fig. 17. The pieces to be joined are

placed in between two graphite rods, 2 inches in diameter. The top rod is static

while a hydraulic system is used to apply pressure on the bottom rod which in

turn applies pressure on the sample. This assembly of graphite rods and sample is

loaded into a vacuum chamber which is cooled by running water in the course of

bonding. A vacuum pump maintains sufficiently low pressure in the chamber

protecting the workpieces against oxidation as they are heated for joining. The

chamber is first evacuated using a mechanical pump to a pressure of 10^{-2} mbar

and then an oil diffusion pump is used to reduce the pressure close to 10^{-5} mbar.

Heat is supplied by the inductor of a high frequency oscillator. When the joint is

completed, the weldment is brought down to the room temperature or specified
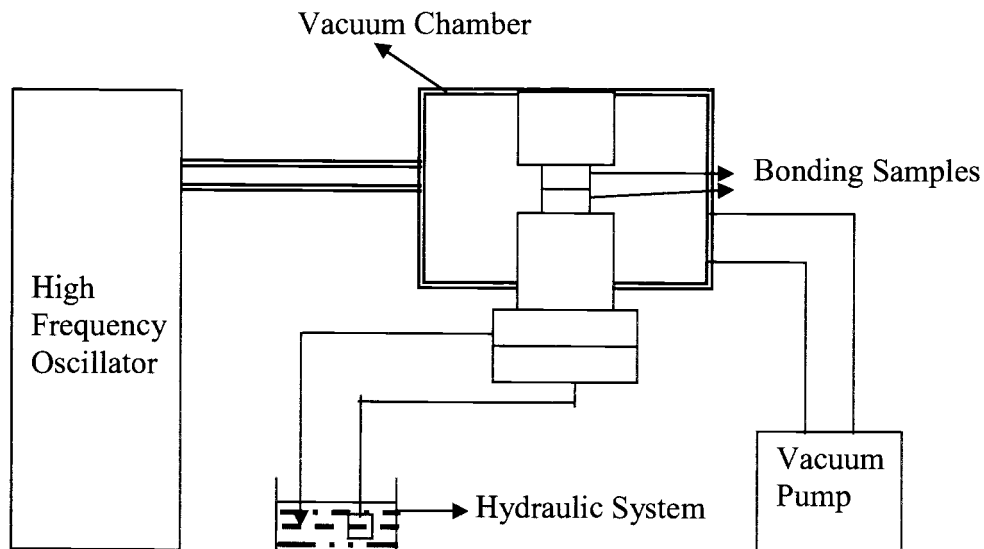
temperature in vacuum.

Figure 17: A block diagram of the hot press with its components.

3.4 Embossing

Six embossing runs were conducted using five different dies which are described in the following paragraphs.

3.4.1 Dies used for embossing

This section describes each die in detail along with the images of the dies.

3.4.1.1 Die#1- Three Channel die

Precision cut pieces of stainless steel 316 were used to make a three channel die which was used for runs 1 and 2. To accomplish this, seven pieces were cut from 100 μm shim stock of stainless steel 316 using a laser. All laminae were polished and deburred with ultra fine 3M Scotch-Brite^{TM} and cleaned in an ultrasonic cleaner afterwards. The patterned and deburred layers were stacked between graphite platens and flattened at a temperature of 773 K and a pressure of 2.4 MPa (350 psi) for 30 minutes which also served to relieve any residual stress from the cold rolling process. All these pieces were 25 mm wide and were cut out of 100 μm stainless steel 316 shim stock. Three of the seven pieces were 15.250 mm high while the other four were 15 mm high. To make the die these pieces were piled alternatively in the hot press and diffusion bonded at 1073 K and under a pressure of 2.4 MPa. It can be seen that on being replicated these would leave three channels in the substrate. The arrangement of the seven pieces is schematically shown in Fig. 18 (a) and (b). Optical micrograph of the side view of the die thus fabricated is depicted in Fig. 18 (c).

(a)   (b)

(c)
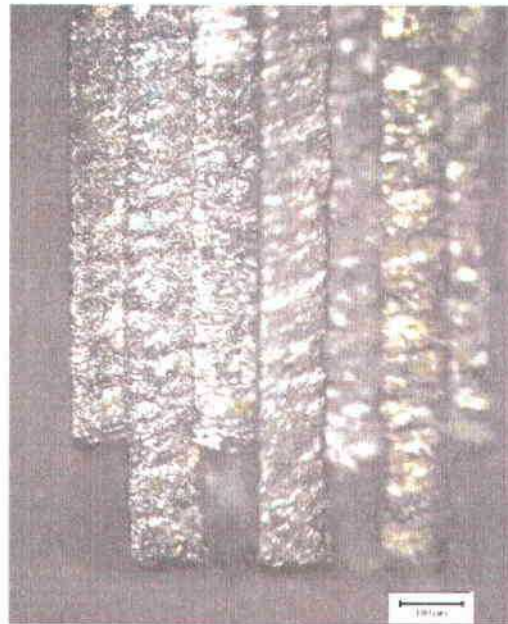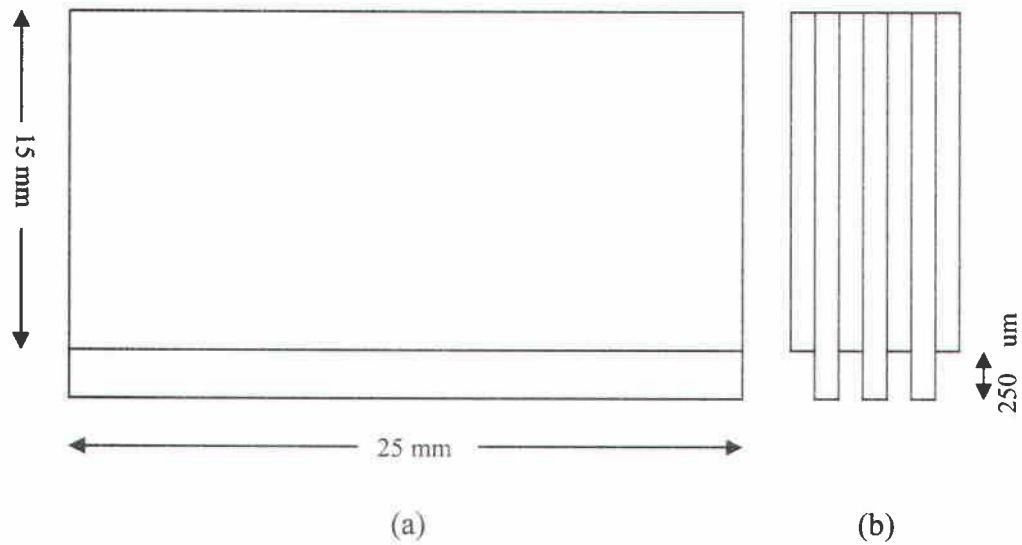
Figure 18: Schematic arrangements of the SS pieces in die#1. a) Front view b)
Side view c) Optical micrograph of bonded die showing side view.
(micron bar = 100 µm)

3.4.1.2 Die#2 – Spiral Die

An oval spring was pressed into a piece of steel at room temperature. The

resulting impression on the steel piece along with its profiler image is shown in an enlarged view in Fig. 19. This was used as the die for run#2.
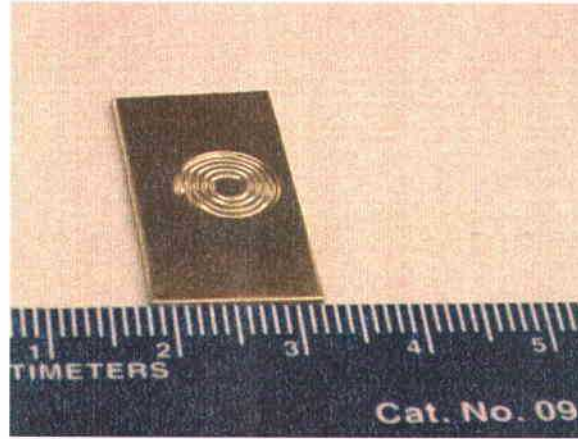
(a)
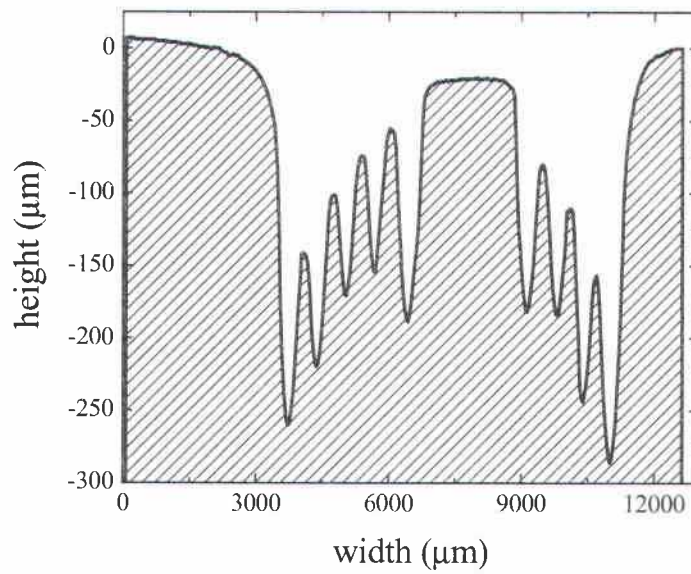
(b)

Figure 19: For Die#2 a) Magnified image b) Profiler graph.

3.4.1.3 Die#3 – US Dime

Figure 20 shows a magnified image of the dime which was used as a die for the
fourth run.

Figure 20: Magnified picture of the dime used for fourth run.

The feature size on a dime varies from 200 µm to 5 µm. In addition to the features
on the dime there were also marks from machining that were replicated on the
Vit4 sample. The various features are illustrated in Fig. 21 below.

10 μm deep ridges
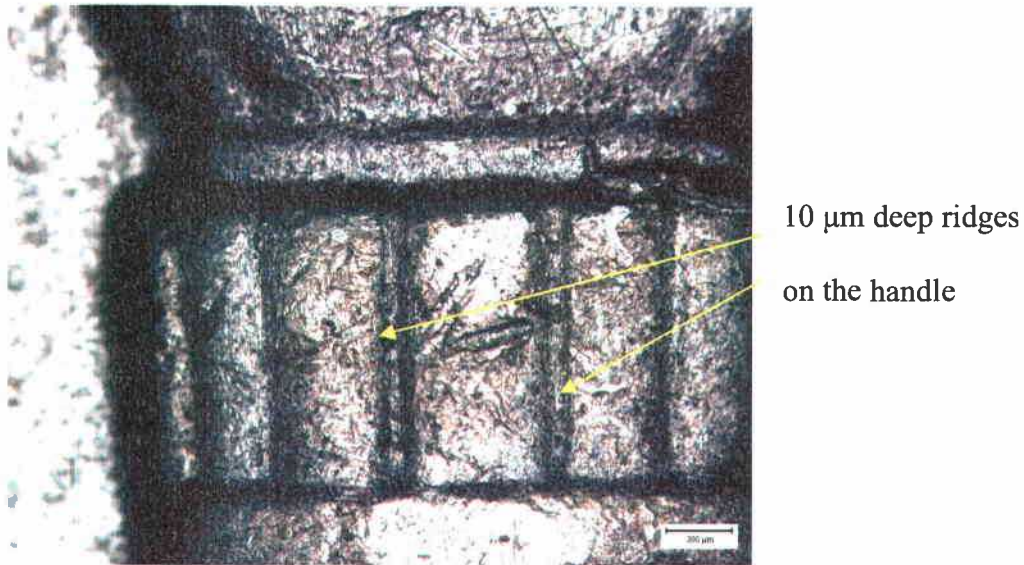
on the handle

Figure 21: Optical micrograph showing the ridges on the handle which is marked as Region II in Fig. 20. Approx depth of the ridges in the center is 10 μm and for those on the sides is 5μm.

3.4.1.4 Die#4 – Fractal Die

Pence D. *et al.* at Oregon State University have developed highly intricate and miniaturized microchannels that are laid out on a piece of stainless steel 38 mm in diameter. The channels originate at the center and branch out into more and more channels thus resulting in fractal geometry. They are approximately 210 μm wide and 35 μm deep. The fourth die used for embossing was a piece of this steel fractal that is shown in Fig. 22 below.
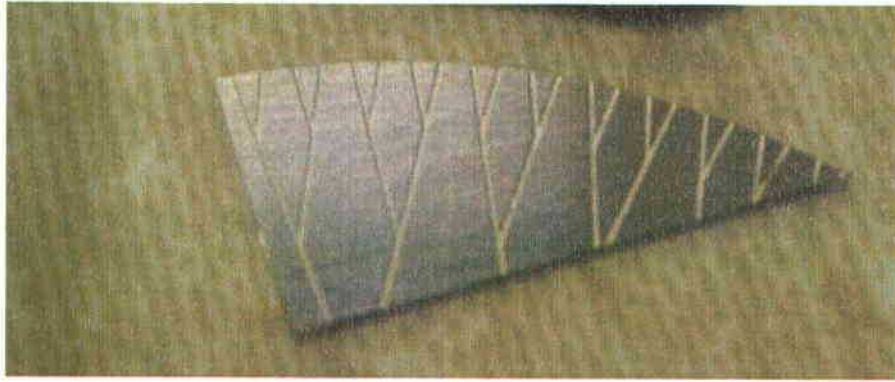
Figure 22: Steel fractal developed at Oregon State University (Courtesy Dr. Pence, OSU).

3.4.1.5 Die#5 – Single Channel Die

Die#5 consisted of one feature which was 1 cm long and 238 μm high. The cross section of this feature was trapezoidal with bigger side of 400 μm and shorter side around 200 μm wide. This die was machined out of stainless steel piece and used as a die for sixth run. Figure 23 shows the magnified view.
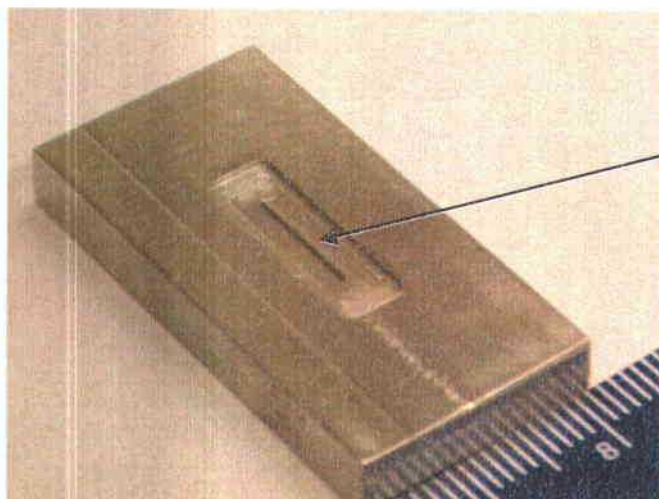
Single feature machined into the steel piece

Figure 23: Photograph of Die #5 showing the feature that was machined in a steel piece.

3.4.2 Embossing Procedure

Temperature, pressure and embossing time were the three main parameters to be determined ahead of each run. As elucidated in chapter 2.2, for temperatures in the vicinity of 650 K, Δh = 500 μm, a = 4.674 mm and F = 890 N, embossing time, Δt, are less than time for onset of crystallization, t_{cry-on}. This range of temperature is also preferred because the corresponding Δt values are most feasible on experimental time scale. Each die was profiled prior to the run and hence the maximum replicable feature size was found and inserted into the Eq. (3) as Δh. Another variable in Eq. (3) is the viscosity, η, which is constant at the embossing temperature. Hence, the embossing times for all runs were determined. For all the runs the sample and the corresponding die were placed such that the polished face was in contact with the die. They were positioned in between the graphite rods of the hot press. A constant heating rate was used to get the chamber to a predetermined temperature and then pressure was applied. The samples were held under these conditions isothermally for a preset time after which they were cooled to room temperature under vacuum. Experimental conditions for all the six embossing runs are listed in Table VII.

Table VII: Experimental conditions for six embossing runs.

Expt. No.	Die	Temp. (K)	Time (s)	Force (N)	Ramp (K/s)
1	Three channels	633	2700	890	0.25
2	Three channels	648	1200	890	0.25
3	Spiral die	633	3600	890	0.167
4	Dime	623	9000	890	0.167
5	Fractal	623	3600	890	0.167
6	Single channel	633	3600	890	0.167

Following the embossing, optical microscopy was carried out on the samples using Leica DMRM optical microscope fitted with Leica DC 300 camera and equipped with Leica IM50 software to which aids in making high magnification pictures. The areas which appeared as replica of the die were then studied with the aid of the profiler. Differential Scanning Calorimetry was also performed to ascertain if the sample crystallized or was amorphous.

3.5 Bonding Procedure

The samples were prepared, polished and profiled as described in chapter 3.1. Two pieces were placed on top of each other with their polished faces in contact, between the graphite platens. The chamber was evacuated to a vacuum of approximately 10^{-5} mbar and heated to a predetermined temperature at a constant heating rate. Pressure was then applied and the samples were held under these

conditions isothermally for a preset time. All the bonding samples were allowed to cool in vacuum and under pressure. The experimental conditions for the bonding cycles are given below in Table VIII.

Table VIII: Experimental conditions for the bonding cycles.

Expt. No.	Temp. (K)	Time (s)	Force (N)	Ramp (K/s)
1	652	9000	890	0.417
2	643	9000	890	0.167
3	643	13600	890	0.167
4	648	10800	890	0.167
5	648	13600	890	0.167
6	648	14400	890	0.167
7	648	16200	890	0.167

The samples which were bonded were embedded in phenolic resin, polished again and analyzed under the optical microscope. DSC revealed if the sample was crystalline or amorphous.

4. Results

All the results for embossing and bonding runs are given in this chapter.

4.1 Embossing

As explained in chapter 3.4.2, after embossing, , every sample was studied under the optical microscope, profiled and then tested for crystallinity using a DSC. Samples from runs 4 and 5 were also studied in Veeco^{TM} Interferometer.

4.1.1 DSC results

The DSC scans for all runs are given in Fig. 24.
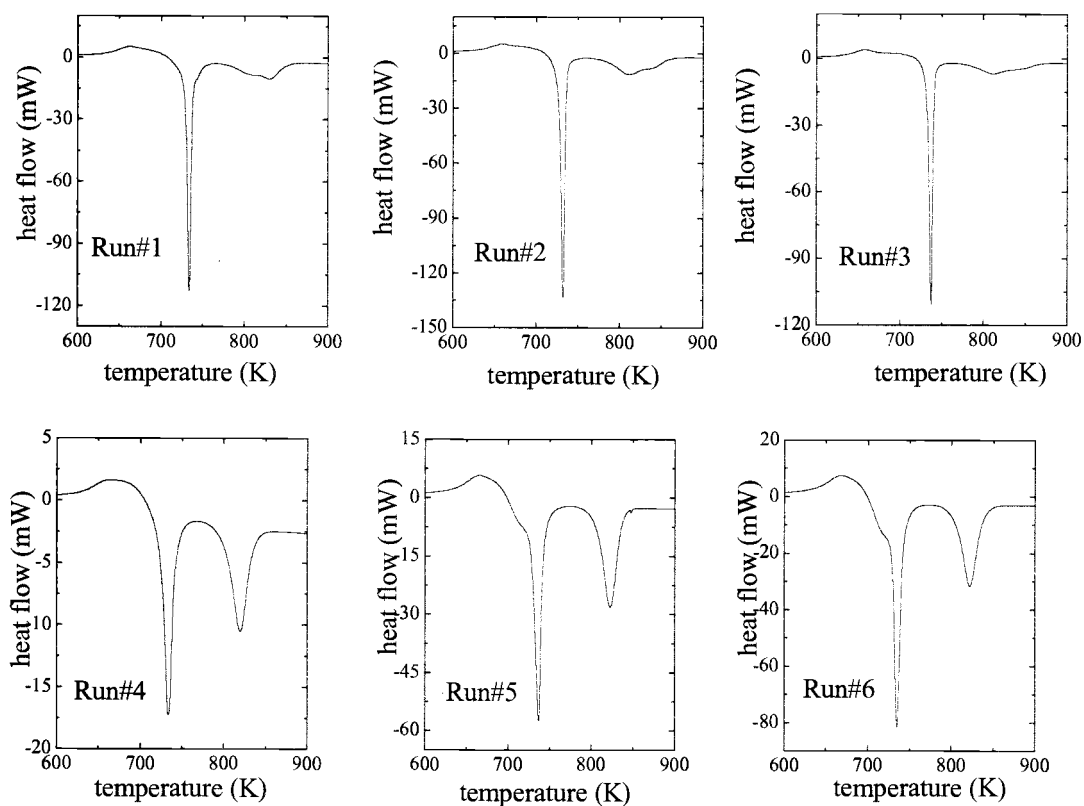
Figure 24: DSC scans for embossing experiments

4.1.2 Microscope and Profiler Images of Embossed samples

The profiling graphs and microscope images for the embossed samples are given below.

4.1.2.1 Run#1- Three channel die

As shown in Fig. 18 above, this die had three vertical features each having a rectangular cross-section, 250 μm high and 100 μm wide. The replicated Vit4 sample underwent a very small amount of deformation. The profiling graph of the sample is depicted in Fig. 25.
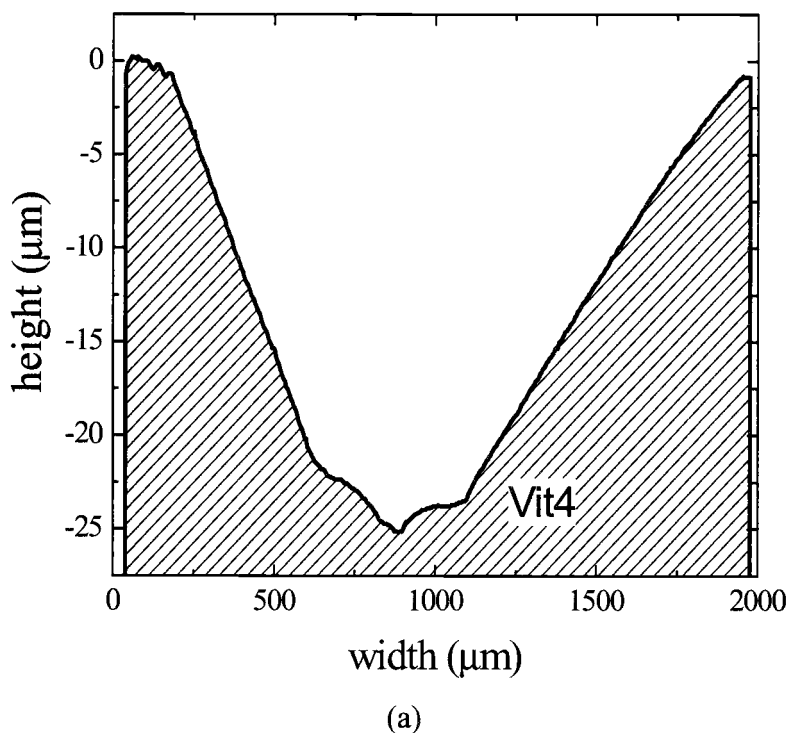
(a)

(b)

Figure 25: Profiling graphs of Run#1 sample (a) Scan of the whole sample.
Microchannels are hardly distinguishable. (b) Closer view of the
microchannels along with their approximate positions shown by dotted
lines.

The features in the die were expected to make three microchannels in the sample.

But what ensued, as seen in Fig. 25 (b), were three depressions which were only

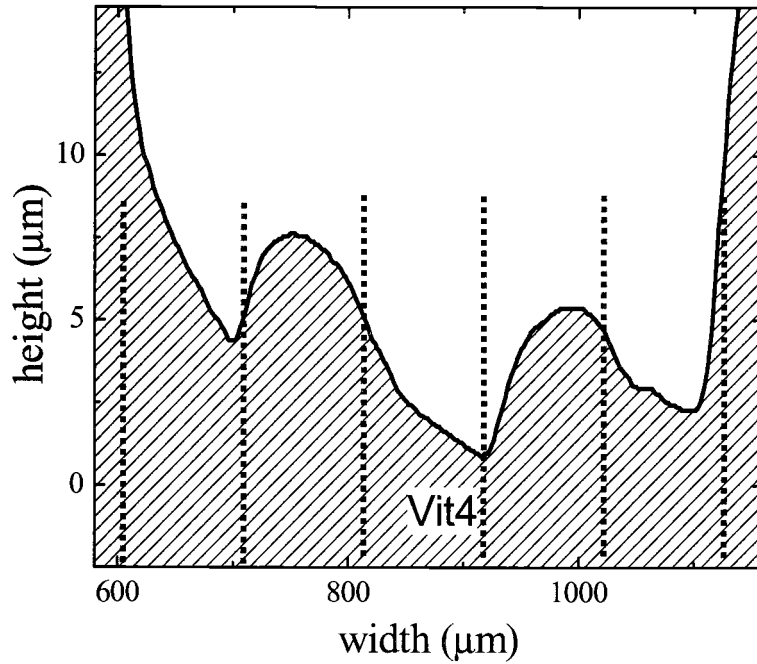about 8 µm deep. The ratio of feature height replicated on the sample to feature

depth on the die is called replication accuracy (R). Hence, R for run#1 was only

3.2 %. It appears from Fig. 25 (a) that the sides have a slope. The maximum depth

from the surface of the Vit4 sample is around 25 µm. This was due to the lack of

control over the furnace temperature. The sample was only heated to 616 K.

4.1.2.2 Run#2 - Three channel die

The three channel die was used again with a higher furnace temperature of 648 K.

The profiling graph of the sample is depicted in Fig. 26.
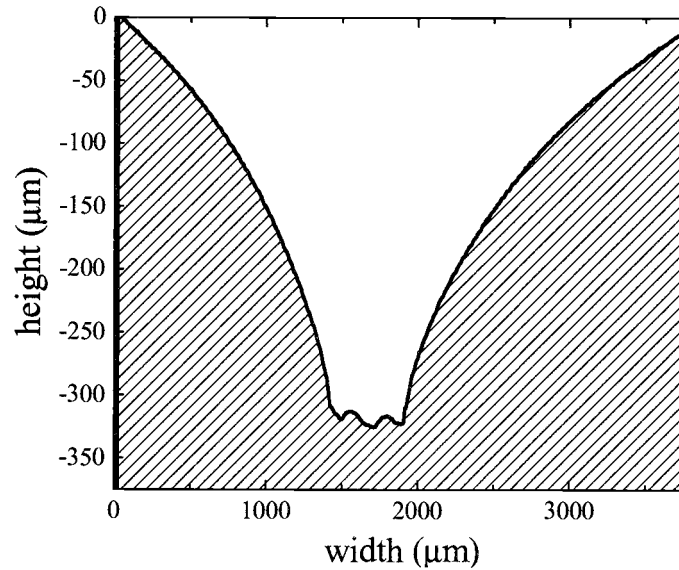
Figure 26: Profiling graph of Run#2 sample.

It is revealed from Fig. 26 that the die could not penetrate the sample and left

three channels which were only around 10 μm deep similar to run#1. But the

maximum depth from the Vit4 surface was around 335 μm, much higher than 25

μm in run#1.

4.1.2.3 Run#3 – A thin steel piece with spiral features.

A thin steel piece with spiral features, depicted in Fig. 19, was the embossing tool.

The profiling graphs of the sample and the spiral die are given in Fig. 27.
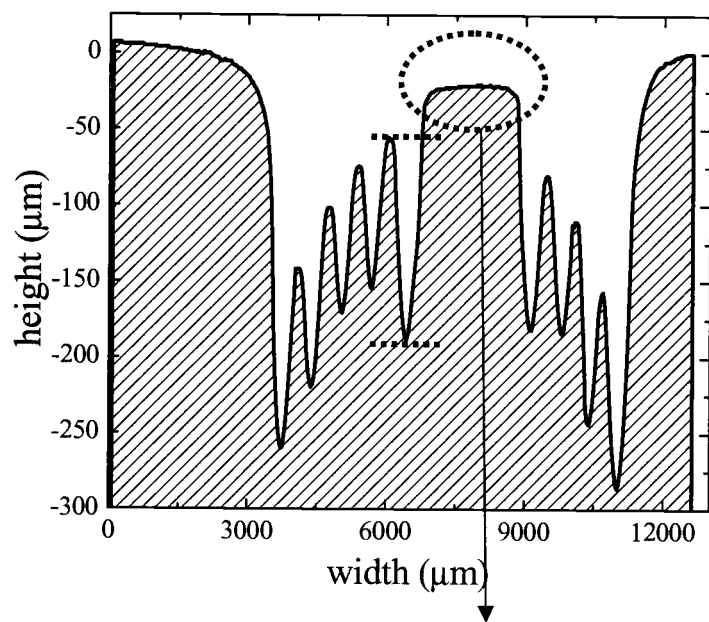
(a)
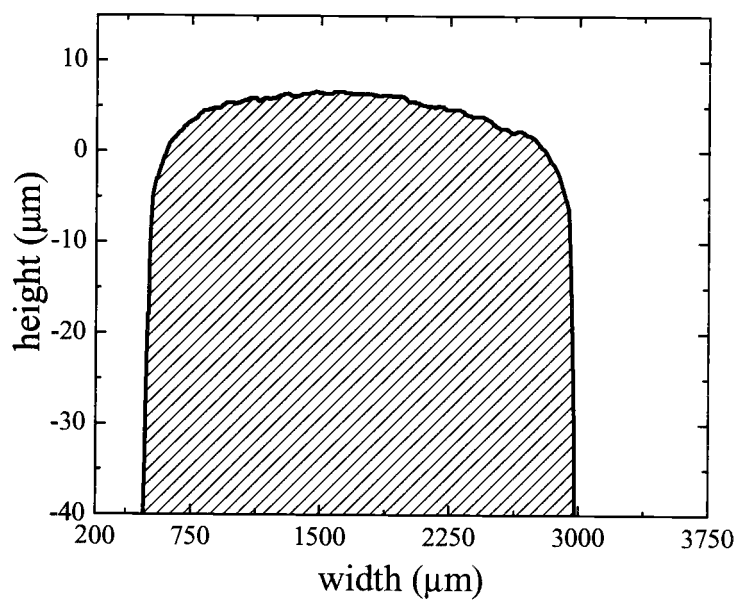
(b)
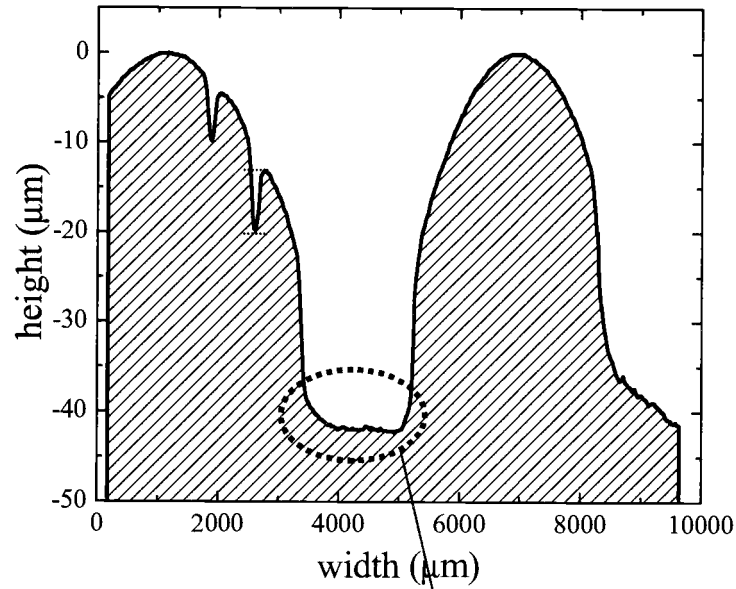
(c)
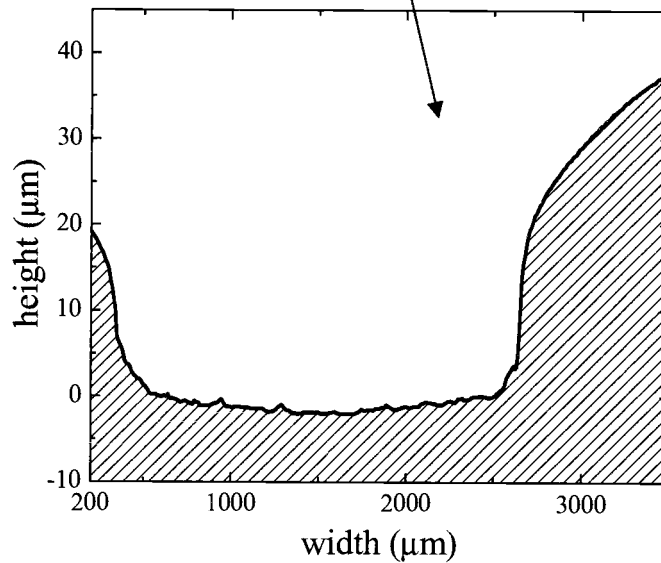
(d)

Figure 27: Profiling graphs of die and sample from Run#3. a) Full scan of die, b) enlarged center portion of the die, c) Full scan of sample, d) Magnified view of the center of the sample.

In this die the feature depth varied from 160 µm to 290 µm. Figure 27 (a) displays a complete profiling scan of spiral die and various features with varying depth can be seen. Figure 27 (b) shows the central section of the die which is 2.4 mm wide

and about 50 μm high. Profile of its replication on the sample is given in Fig. 27 (d). It is clear that the sides of the replicated feature are curved and not vertical. The width at the bottom of the feature is about 2.5 mm and the depth is about 42 μm. For the narrower and deeper features, the replica on the sample is either missing or if present is far less than expected. For example, one such feature is marked using dotted lines in Fig. 27 (a). This feature is 130 μm deep, but it is replicated as a peak only 8 μm high which is marked on Fig. 27 (c) using horizontal dotted lines. The ratio of the height to width of the feature is called aspect ratio. Thus, for the high aspect ratio features, that is the narrower and deeper features, R= 6 %, while for low aspect ratio features R = 88 %.

4.1.2.4 Run #4- Dime

Optical micrographs of the embossed piece of Vit4 at various magnifications are given below in Fig. 28 . Also shown are the corresponding sections on the coin.

(a)

| (b) | (c) |

| (d) | (e) |
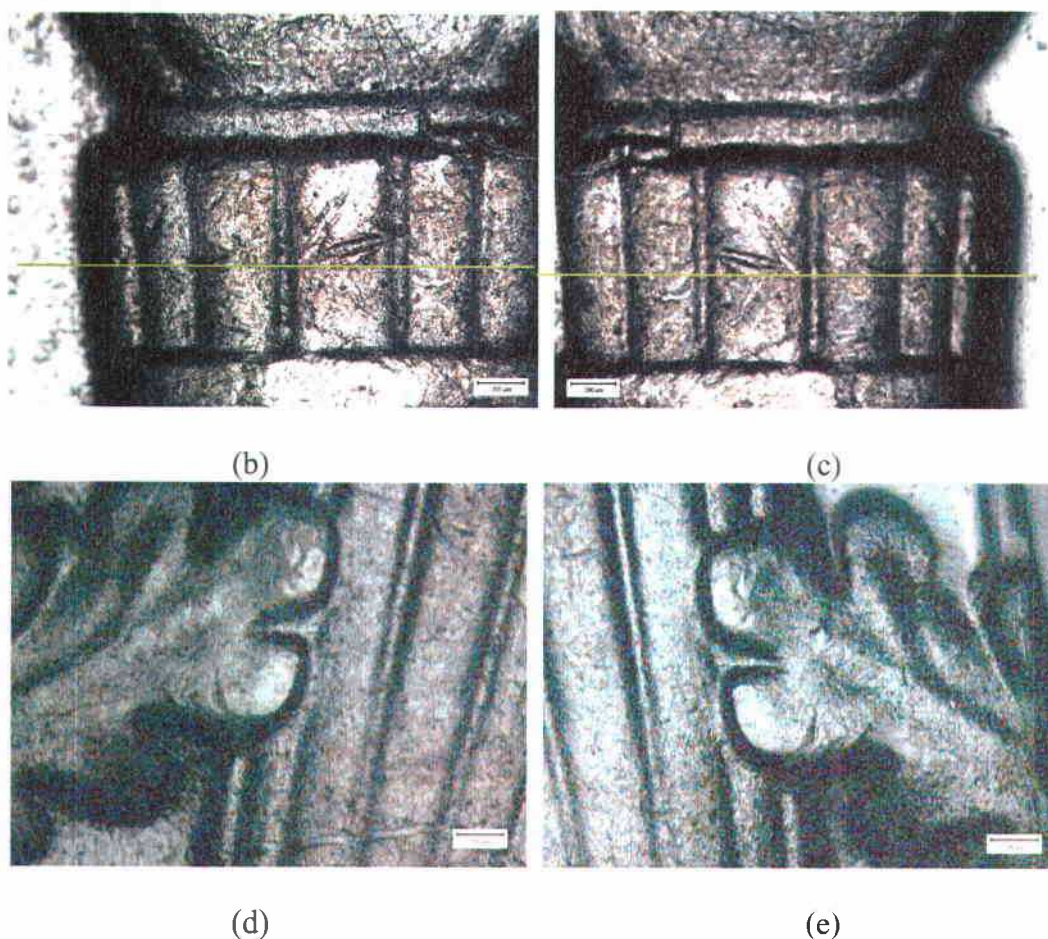
Figure 28: Optical micrographs of Run#4 sample a) Enlarged view of the coin and the sample, b) flame handle with its ridges on the coin, (c) replicated portion on the sample, d) oak leaf on the coin, and (e) the same replicated on the sample. Note that the images in (c) and (e) are depressed into the surface of Vit4. The orange lines in (b) and (c) show the approximate positions where the profiling scans, given in Fig. 29, were done.

The features of the coin such as the flame, the ridges on the handle and the oak leaf have been replicated successfully. The accuracy of replication is revealed by looking at the profiling graphs of various areas on the sample and the matching sections on the coin. One such comparison between the handle of the flame on the dime and corresponding imitation on the sample is depicted in Fig. 29. The

approximate positions where profiling was carried out are marked with orange

lines in Fig. 28 (b) and (c).
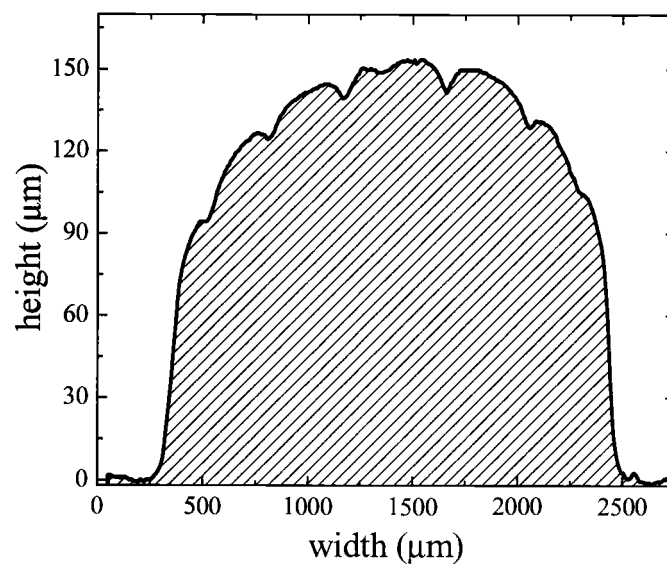
(a)
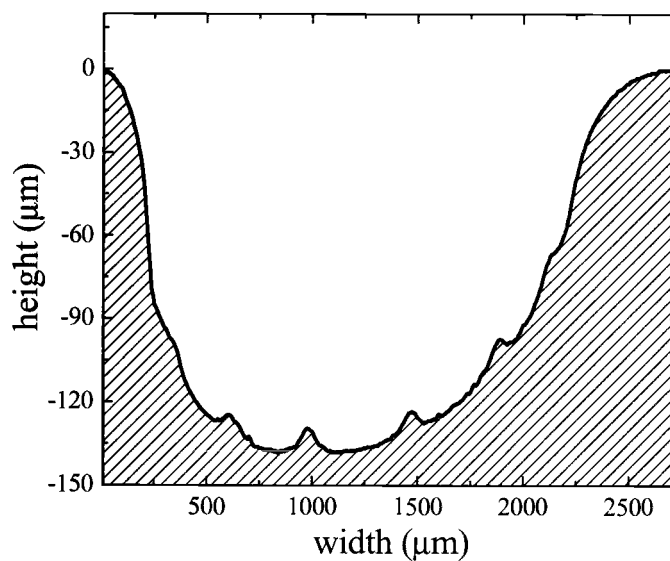
(b)

Figure 29: Profiling graphs of (a) handle on the coin, and (b) related area on the sample.

The handle of the flame on the dime has a maximum height of about 150 μm at

the center. The corresponding depth on the sample is only 140 µm. Therefore, for

run#4, R = 93.3 %. Veeco interferometer pictures for the flame on the dime

(Region I in Fig. 20) and the same replicated on the sample are given in Fig. 30.
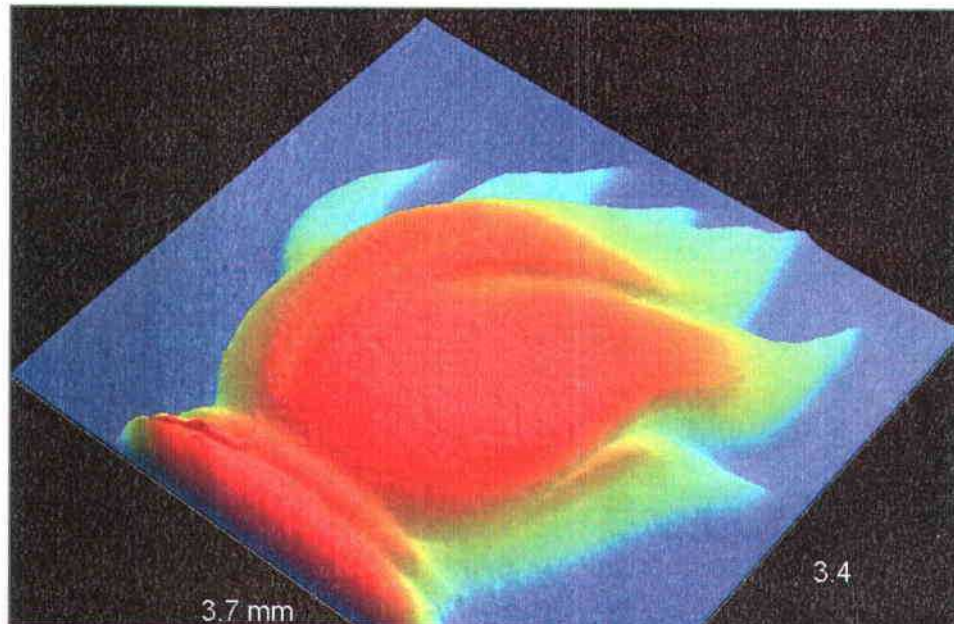
(a)
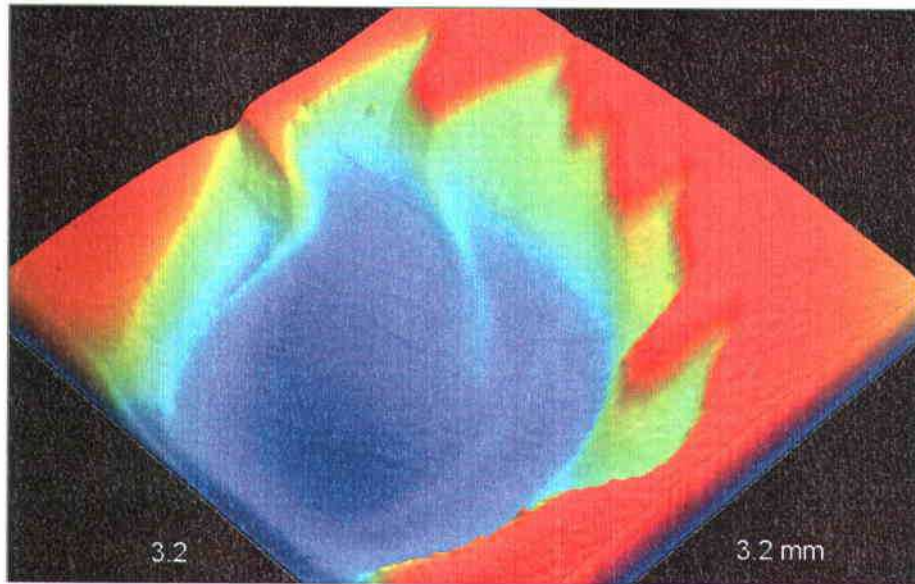
(b)

Figure 30: Interferometer images of (a) flame on the coin (area scanned is 3.7 mmx3.4mm), (b) replica on the sample (area scanned is 3.2 mmx3.2 mm).

4.1.2.5 Run#5 – Fractal

A stainless steel disc with fractals etched on it was used as the die. Photograph of the fractal and the Vit4 sample with replicated features is shown in Fig. 31.
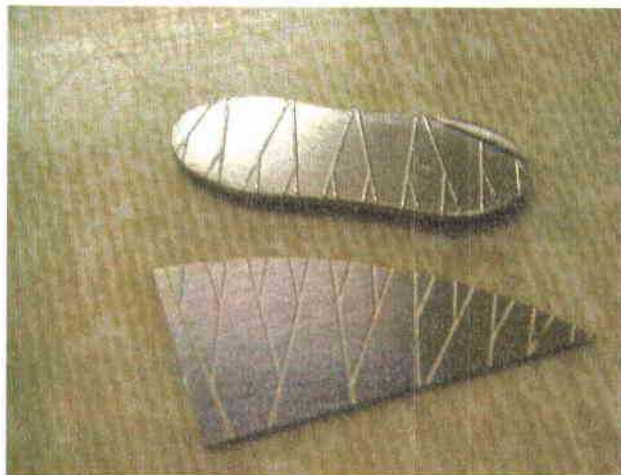
Figure 31: Photograph of the fractal and the replicated sample.

The profiling graphs of the microchannels on the die and sample are portrayed in Fig. 32.
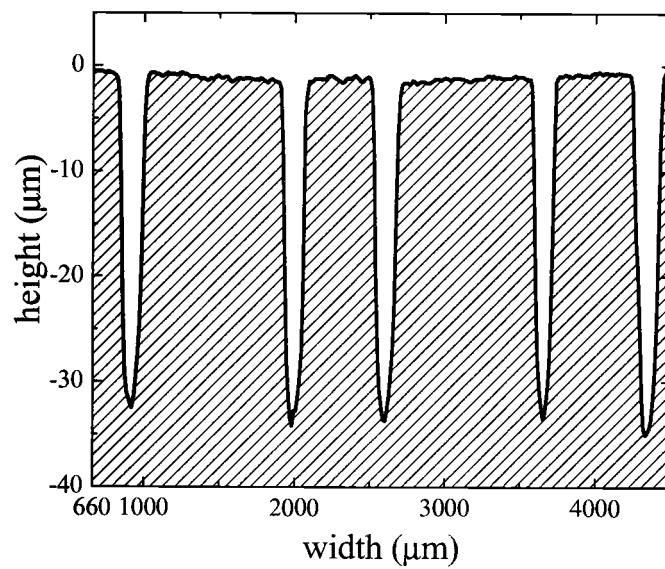
(a)
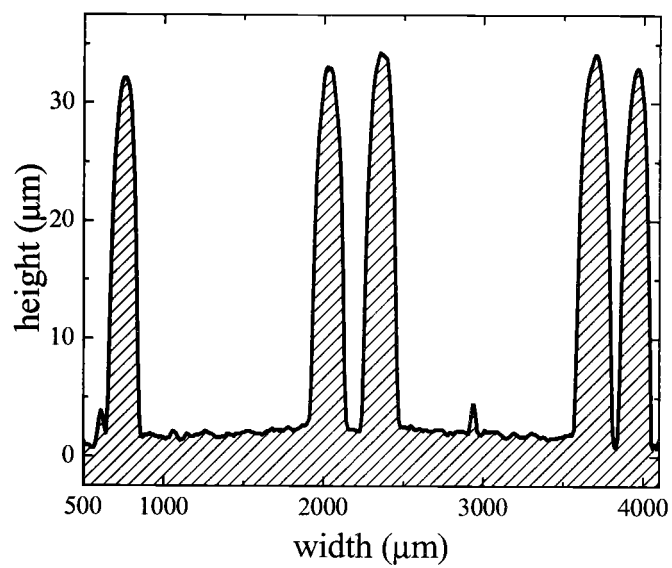
(b)
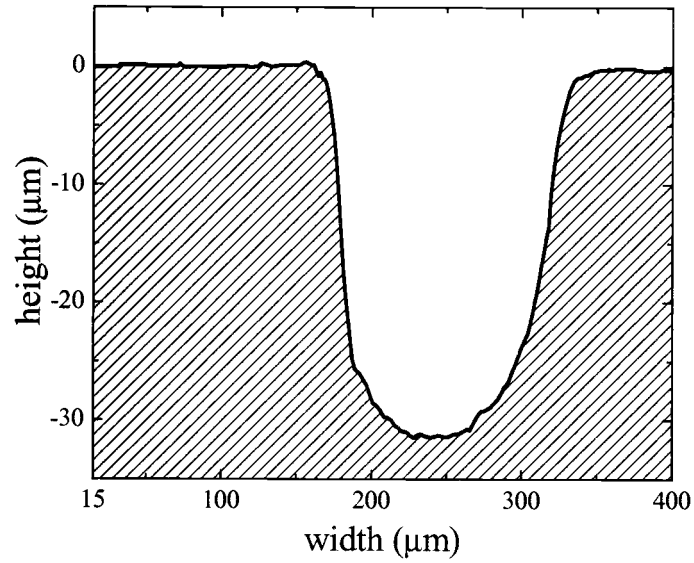
(c)
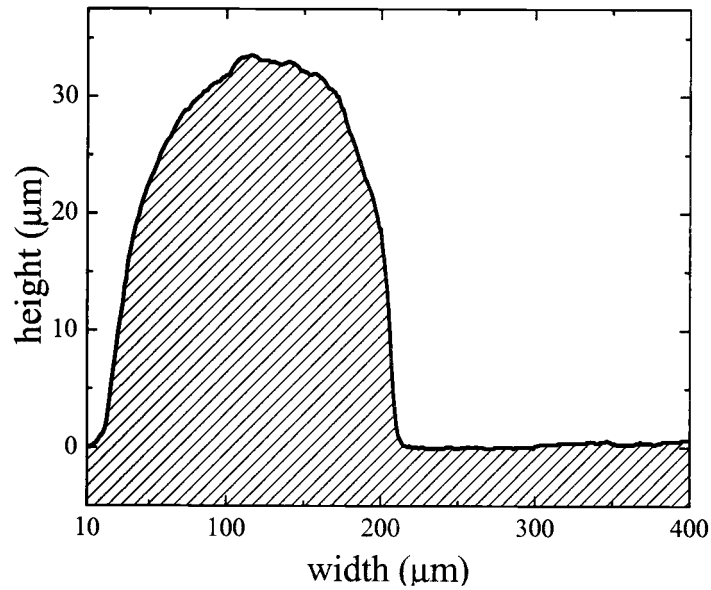
(d)

Figure 9: Profiling graphs of Run#5 die and sample a) Channels on the fractal,
b) Replicated peaks on the sample, c) Single channel on the fractal,
d) Replicated single peak on the sample.

Interferometer images of the die and replicated sample are shown in Fig. 33.
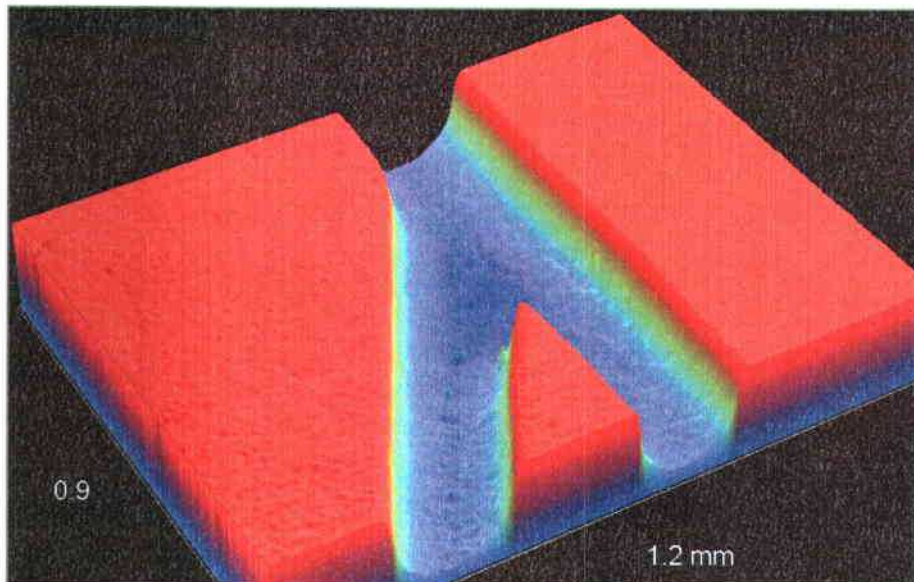
(a)
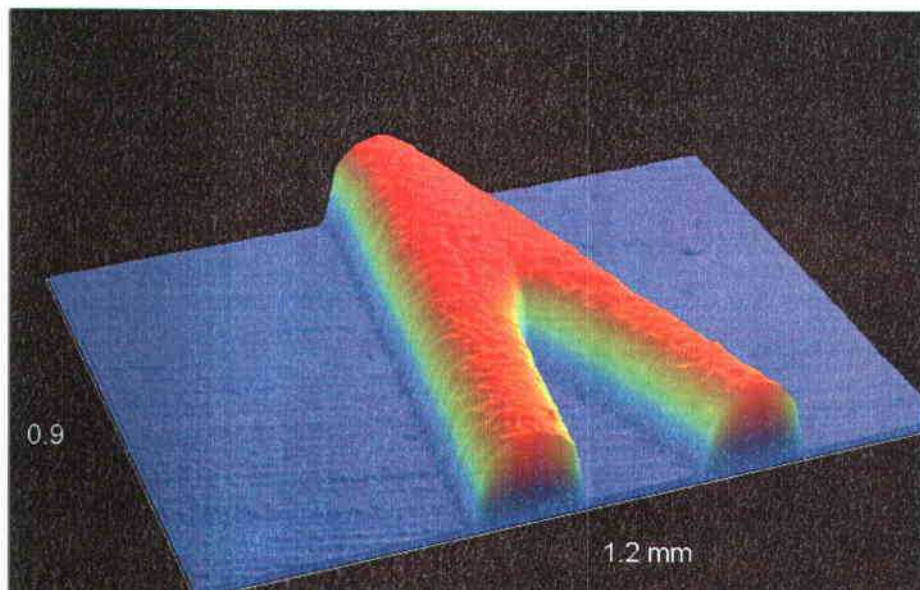
(b)

Figure 33: Interferometer images taken at 5x magnification
(a) microchannel in the die (area scanned is 0.9 mmx1.2 mm),
(b) replication on the sample (area scanned is 0.9 mmx1.2 mm).

The average depth of microchannels on the die is 37 μm and the average height of

replicated features on the sample is 36 μm. This yields R = 97.3 %.

4.1.2.6 Run#6 – Single channel die

Enlarged images of the die and the embossed piece of Vit4 are shown in Fig. 34.

Also shown are optical micrographs of the cross section of the embossed piece.
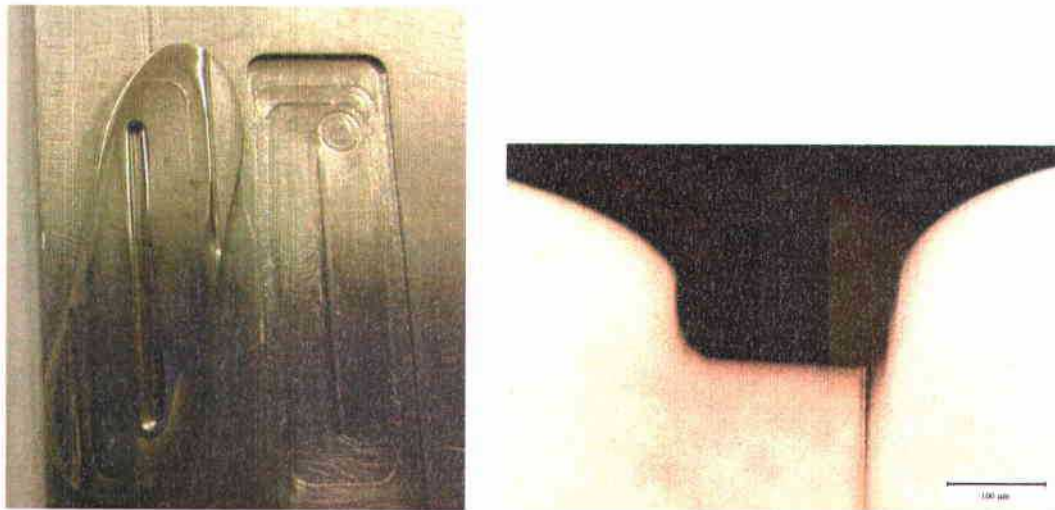
(a)   (b)

Figure 34: a) Enlarged view of the die and BMG sample,
b) Optical micrograph of the cross-section of the embossed
microchannel.

The profiling graphs of the sample and the die are depicted in Fig. 35.
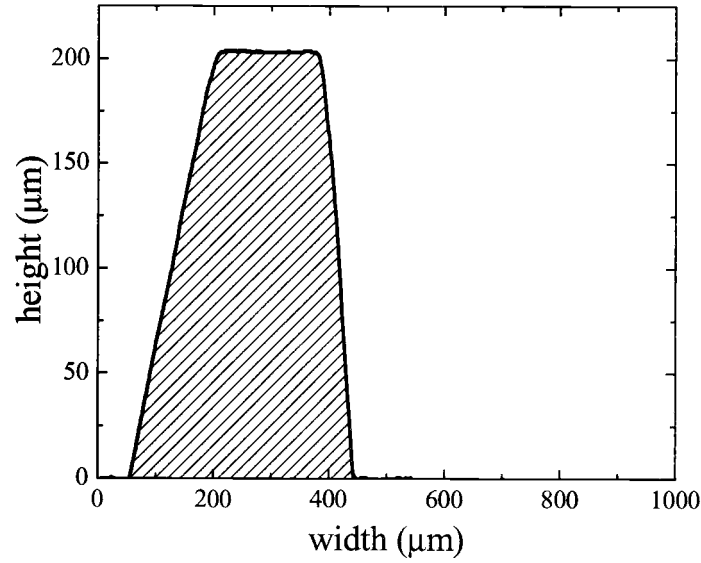
(a)
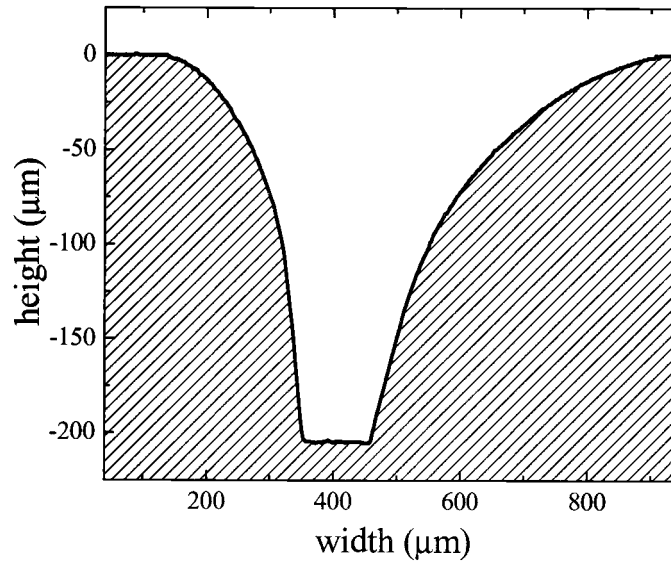
(b)

Figure 35: Profiling graphs of a) Single channel die, b) Run#3 sample.

The die has a single feature which is about 238 µm high. The cross section of the feature is not a rectangle but a trapezium with the small side 180 µm long and large side about 400 µm long. This is evident from Fig. 35 (a). The replicated microchannel on the Vit4 sample is approximately 230 µm deep but the small side

of the trapezium is only 140 μm long while the long side is 750 μm. The vertical

sides of the trapezium in the replicated microchannel are not straight but curved.

This is also seen from the optical micrograph of the sample in Fig. 34 (b). The

depth to height ratio, R, is 97 %.

4.2 Bonding

Table VIII, in chapter 3.4.2, lists the experimental conditions for all the bonding

experiments. As the bonding conditions were changed the samples either turned

out to be weakly or strongly bonded. For run#2, the two pieces of Vit4 were

apparently bonded but did not hold together and hence the bond in this case

turned out to be a weak bond. The samples in rest of the experiments were

permanently bonded and hence it was possible to carry out the optical microscopy

on these samples. The micrographs, for the six bonded samples are given in Fig.

36 below.
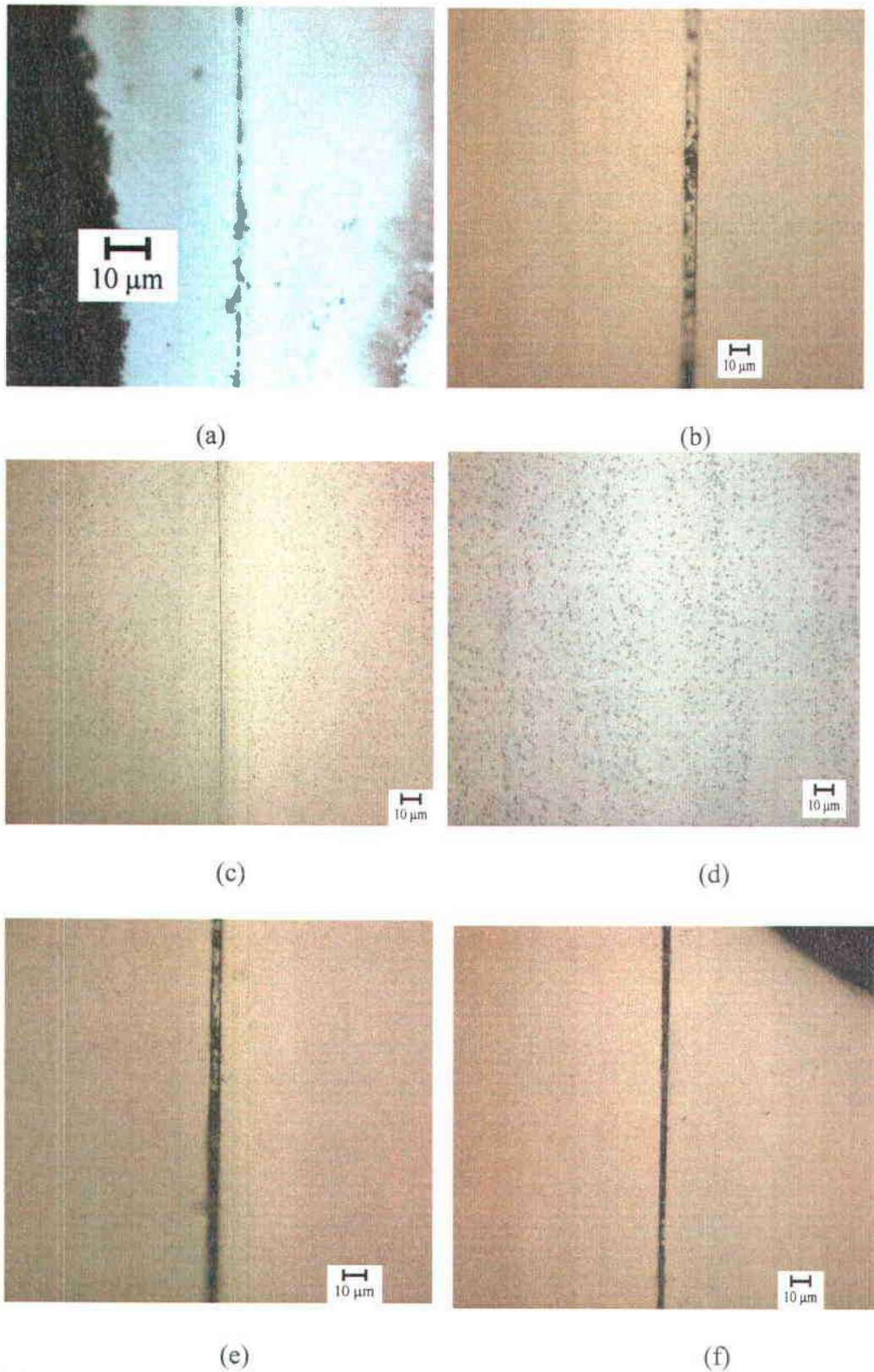
Figure 36: Micrographs of the bonded samples. (a) to (f) correspond to run#1 to run#7 respectively, barring run#2.

DSC scans for all the samples are depicted in Fig. 37.
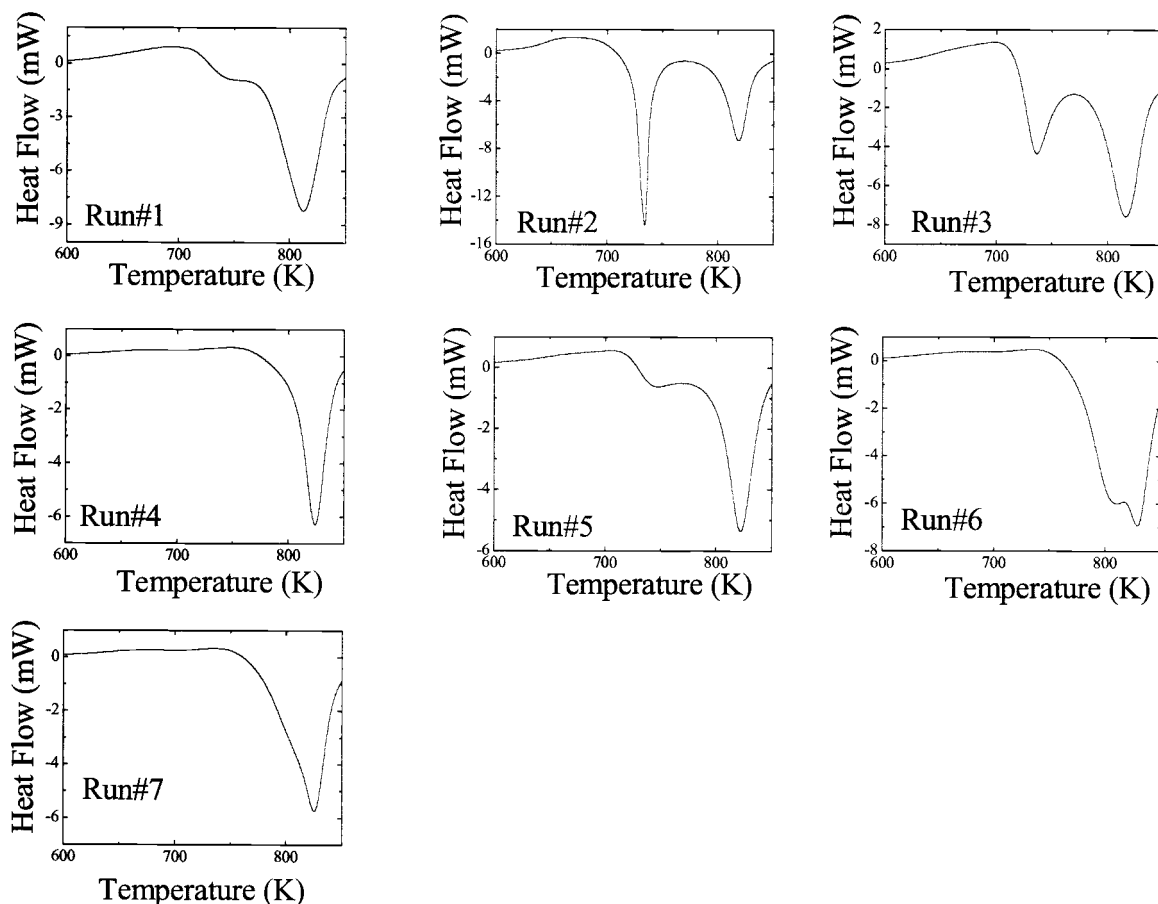
Figure 37: DSC plots for all the boding samples.

Except for run#2 all other samples were crystalline. Sample in run#2 underwent a

phase separation which is clear from the two peaks in the DSC plot for this

sample. C values for all the samples calculated from the DSC plots are given in

Table IX.

Table IX: C values for the bonded samples.

Run#	Type of Bond	% crystallinity, C
1	Permanent	33
2	Weak	0
3	Permanent	42
4	Permanent	17
5	Permanent	12
6	Permanent	17
7	Permanent	12

5. Discussion

5.1 Embossing

Temperature, holding time and pressure were the three important parameters for both embossing and bonding. These were estimated using the VFT plot (Fig. 10), the TTT diagram (Fig. 11) and Stefan equation (Eq. 3). The experimental conditions for the six embossing runs are given in Table VII above.

5.1.1 DSC analysis

It was mentioned in chapter 2.1, that Vitreloy 1^{TM} undergoes phase separation when heated up close to the T_g. Vit4 also undergoes phase separation but only when annealed for long times at temperatures close to T_g. This phenomenon is seen in the DSC scans of the six embossing runs shown in Fig. 24 in section 4.1.1. For the first three runs the time and temperature were both This is depicted with the help of a schematic TTT curve for phase separation in Fig. 38 below. Also, there seems to exist a critical temperature, T_c, above which the material will not decompose. This implies that at temperatures lower than T_c, Vit4 will decompose on annealing. Hence two peaks are observed in the last three scans of Fig. 24. Each peak corresponds to the crystallization of one particular phase. Larger annealing times result in a larger decomposition of Vit4. This is evident from the last three plots of Fig. 24 where prolonged annealing facilitated long range diffusion and hence the material could decompose into two phases with relatively different compositions, thus leading to large second crystallization peaks.

Similarly, the comparatively small second peaks in the first and third scans can be attributed to shorter holding times that do not give the atoms enough time to arrange into separate phases. In the second run the temperature was significantly higher than all the other runs and more than the proposed T_c. Hence we do not see any phase separation. A more thorough study is required to probe the TTT for phase separation.

5.1.2 Replication Accuracy

It is found that R is a very strong function of viscosity which in turn varies exponentially with temperature. The values of R for all the experiments are listed below in Table X.

Table X: R for various embossing runs.

Run#	Die	Target T	Actual T	Replication Accuracy, R
1	3 channel	633	616	3.2
2	3 channel	648	643	4
3	Spiral	633	618	88 and 6
4	Dime	623	623	93.3
5	Fractal	623	623	97.3
6	Single	633	630	97

For the first run, the three projections in the die shown in Fig. 18, hardly produced any mark on the Vit4 piece, shown in Fig. 25. The chamber of the hot press was heated to a temperature of 633 K (360 °C) and maintained at this temperature for

2700 s (45 min). The calculation from Eq. (3), suggested a deformation of around

250 μm. But instead the maximum deformation obtained was only 25 μm. This

meant that the actual temperature the furnace reached was only 616 K (343 °C).

Hence, the sample was 17 K below the target temperature. The temperature for

the next run was increased to 648 K (375 °C). The embossing time for this run

was only 1200 s. This produced a sample with a poor R of 4 %. Even though the

depth from the surface of Vit4 in this case was 335 μm, as shown in Fig. 26, the

individual channels embossed in the glass piece were only around 10 μm deep.

Using Δh = 335 μm, the temperature was back calculated from the Eq. (3) and

found to be 643 K (370 °C). Hence, for run#2 the sample was 5 K below the

target temperature. Similarly using the final deformation to back calculate final

temperature for the third run, gave the final temperature of sample as only 618 K.

This implied that for run#3, the sample fell short of the target temperature by 15

K. But the holding time of one hour meant that the material still had enough time

to flow into the wide depressions in the die. The R for the wide feature in the

center of the die was about 88 %. But higher viscosity still resulted in

unsatisfactory reproduction of high aspect ratio narrow features, with R = 6 %.

The last three embossing runs have much higher values for R. The features on the

coin, the fractal and the single channel die were replicated with high precision,

but the DSC plots revealed the sample underwent phase separation. This is not

desirable because of the loss of strength associated with phase separation.

Equation 2 shows that the viscosity of Vit4 is highly temperature dependent. For

example, the viscosity at 638 K is $2.45*10^9$ Pa.s, at 643 K it is $1.36*10^9$ Pa.s

while at 648 K it is $7.76*10^8$ Pa.s. This translates into a deflection of 30 μm, 50

μm and 100 μm at these temperatures respectively, with embossing force, F =

890N, radius of the substrate, a = 4.673 mm, initial height of substrate, h = 1 mm

and an embossing time of 180 s. Therefore it is necessary to have very good

control over the sample temperature which was missing in the present setup.

In order to put the experimental conditions for embossing in the perspective they

are plotted with uniform deformation curves of Fig. 12, as shown in Fig. 38. This

plot shows the region which was probed by the experiments performed in this

study. It is clear that all the samples are amorphous and that runs 2, 4, 5 and 6

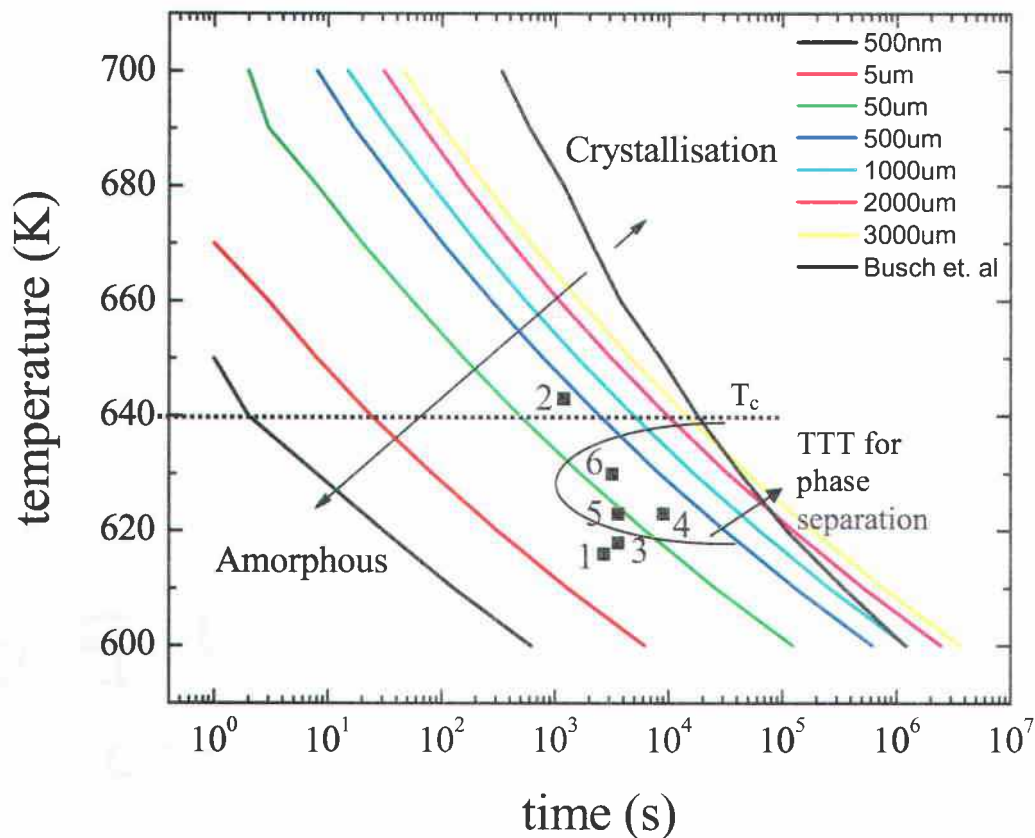showed enough deformation of the sample.

Figure 38: TTT and uniform deformation curves with the experimental conditions
of embossing runs.

Runs 1, 2 and 3 were performed at either low temperature for long times or at high temperature for short times. For both the situations phase separation did not take place in Vit4. This is shown in Fig. 38 with the help of a schematic TTT for phase separation. The dotted horizontal line at 640 K depicts a critical temperature, T_c, above which phase separation is not believed to occur. This phenomenon can be compared to the miscibility gap in the phase diagram of a binary system where the two solids due to their positive heat of mixing like to form two different phases below a certain temperature.

With the equipment used in this research it was not possible to control the temperature of the sample very accurately. But these experiments provide ample testimony to the fact that Vit4 is a good substrate material for embossing of micron level features.

5.2 Bonding

The temperature for the first bonding run was 660 K and the holding time was 9000 s (2.5 hrs). This resulted in a brittle sample with C = 33 %. To avoid crystallization the temperature for the next run was reduced to 643 K while the holding time was still 9000s. This time although the sample turned out to be amorphous, the DSC showed two crystallization peaks which indicated decomposition of the sample. Also the reduction in temperature meant that the diffusivity of atoms in the BMG was less and hence the bond established between the two BMG pieces was very weak. When the sample was being loaded to be cut for DSC measurements, the two pieces just fell apart. For the third run, the sample

was heated to 643 K and was kept there for 12600 s (3.5 hrs). Now the atoms had more time available for diffusion. As a result a permanent bond was obtained as shown in Fig. 36. But the DSC revealed that the sample was crystallized with $C = 42$ %. At this point a time-temperature window for producing a bonded sample was established. The next four experiments were aimed at performing bonding without crystallization. Hence, the bonding temperature was fixed at 648 K while bonding times were increased from 10800 s (3 hrs) to 16200 s (4.5 hrs) in steps of 1800 s (30 min). As mentioned in chapter 5.1, the temperatures were again off the target temperature. The Table XI below shows how much temperature variation was there in each run and also the C value for each run. The onset of crystallization times for actual and target temperatures are also given.

Table XI: Variations in the hot press temperature from the target temperature and C values for all the bonding runs.

Run #	Target T (K)	Actual T (K)	Bonding time (s)	t_{cry-on} (s) for Target T	t_{cry-on} (s) for Actual T	C %
1	652	660	9000	9710	5128	33
2	643	652	9000	20105	9711	0
3	643	657	12600	20105	6509	42
4	648	655	10800	13402	7636	17
5	648	652	12600	13402	9711	12
6	648	651	14400	13402	10523	17
7	648	649	16200	13402	12363	12

Figure 39 is obtained by plotting the times and temperatures for bonding experiments with uniform diffusion length curves obtained in chapter 2.3.5 above.
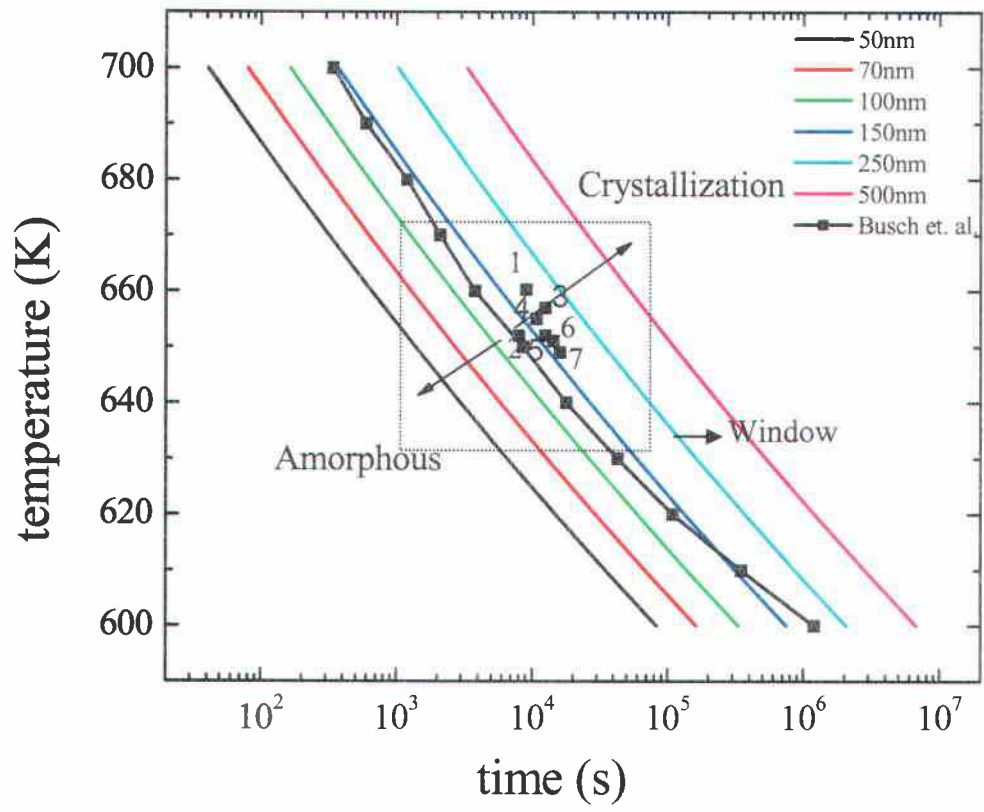
(a)
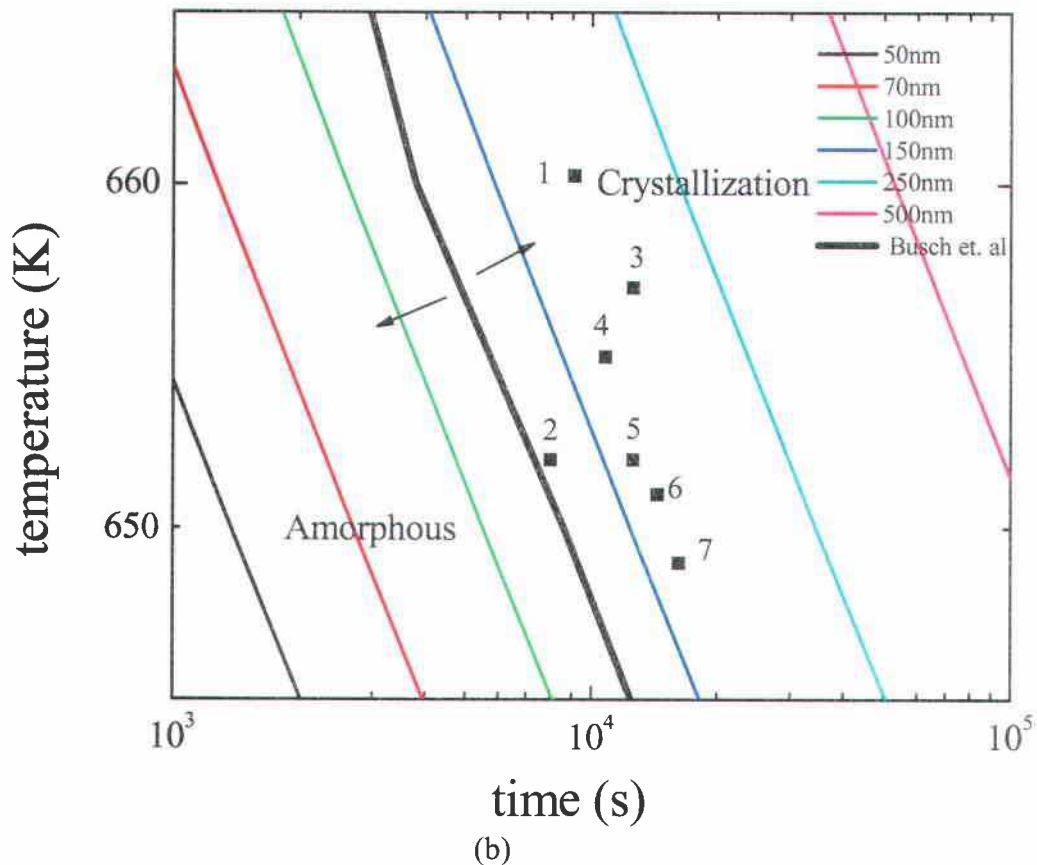
Figure 109: Experimental conditions for bonding on the TTT diagram along with uniform deformation curves for Vit4. (a) the complete TTT curve, (b) time-temperature window that was probed in this research.

Points depicting runs 1 and 3 are well inside the crystallization region while those representing runs 4 to 7 are closer to the crystallization line due to which they are only 10 to 20 % crystalline. The weak bond in the sample from run#2 implies that the 150 nm Ni diffusion length was too small to establish a permanent bond. For the remaining samples, permanent bonding was accompanied by varied degree of crystallization. It can thus be stated that bonding only works if crystallization is tolerated.

6. Summary and Conclusions

MEMS and MECS devices are gaining importance and their effective operation requires materials with the ability to be formed into parts with micron and sub-micron level features. This study focuses on the embossing of micron level features and bonding of the bulk metallic glass forming alloy $Zr_{46.7}Ti_{8.3}Cu_{7.5}Ni_{10}Be_{27.5}$ (Vit4).

Onset of crystallization times for Vit4 were measured by DSC experiments and found to be in good agreement with those measured by Busch *et al.* [24]. Viscosity (η) of Vit4, in the vicinity of its glass transition, measured by Busch *et al.* [24] was used in conjunction with the Stefan equation, Eq. 3, to estimate the time required (Δt) for a fixed deformation (Δh) of a Vit4 piece. The sample thickness (h) and applied force (F) were held constant. A time-temperature window accessible on the experimental time scale was probed by embossing Vit4 substrates using five different dies. Replication accuracy as high as 97% was achieved. The flame feature on a US dime, which was approximately 3mm wide and 150 μm high, and the microchannels in the fractal obtained from Dr. Pence (OSU), which were 200 μm wide and 35 μm deep, were successfully embossed on Vit4 samples.

Diffusivity, D, of different species in a BMG like Vit4 varies inversely to the atomic size of the diffusing species. At high temperatures this difference is not significant. But close to the glass transition, Knorr *et al.* [33] have found that diffusivities for the components of Vit4 deviate significantly. Using values of D

for Ni and assuming Al diffusion to mimic Ti diffusion, the diffusion lengths for Ni and Ti are calculated with the aid of Eq. (4). It is found that Ni diffusion of around 150 nm or Ti diffusion of around 40 nm coincides with the onset of crystallization of Vit4 for temperatures between 600 K and 700 K. It was investigated whether 150 nm of Ni diffusion would be sufficient to obtain a strong bond between the Vit4 pieces. Bonding experiments were performed at temperatures around 648 K. The onset of crystallization time at these temperatures is around 13,500 s (3.75 hrs) and is experimentally feasible. The bonding runs which yielded a permanent bond were unfortunately also crystallized. The experimental conditions which gave an amorphous sample failed to give a strong bond. A minimum crystallinity of 12 % was present for all the bonded samples. Thus bonding could be achieved but not without partially crystallizing the sample. Hence, Ni diffusion of more than 150 nm is required to achieve a strong bond between the samples.

BIBLIOGRAPHY

[1]   A. Lal and J. Blanchard, IEEE Spectrum (Sep. 2004), 38.

[2]   W. Clement, R. H. Willens, and P. Duwez, Nature 187 (1960), 869.

[3]   A.L. Drehman, A.L. Greer, and D. Turnbull, Appl. Phys. Lett. 41 (1982), 716.

[4]   H.W. Kui, A.L. Greer, and D. Turnbull, Appl. Phys. Lett. 45 (1984), 615.

[5]   A. Peker and W.L. Johnson, US Pat. No. 5,288,344 (February 1994); A. Peker PhD dissertation, California Institute of Technology, 1994.

[6]   http://www.memsnet.org/mems/what-is.html, 28th October, 2004.

[7]   http://www.appliedmems.cc/htmlmems/pdf/SF1500L.pdf, Si-Flex^{TM}, 24 October (2004).

[8]   R.S. Benson and J.W. Ponton, Trans. IChemE, 71, Part A (1993), 160.

[9]   W.A. Little, Advances in Cryogenic Engineering, 35 (1990), 1325.

[10]   P.B. Koeneman, I.J. Busch-Vishniac and K.L. Wood, J. MicroElectroMechanical Systems, 6(4) (1997), 355.

[11]   D. Grewell, A. Mokhtarzadeh, A. Benatar, C. Lu and L.J. Lee, ANTEC (2003), 1094.

[12]   L. Klintberg, M. Svedberg, F. Nikolajeff and G. Thornell, Sensors and Actuators A 103 (2003), 307.

[13]   I. McCracken and R. Busch, Master Thesis, I.A. McCracken, (June, 2003)

[14]   S. Schneider, U. Geyer, W.L. Johnson and P. Thiyagarajan, unpublished.

[15]   U. Geyer, W.L. Johnson, S. Schneidr, Y. Qui, T.A. Tombrello and M.P. Macht, Appl. Phys. Lett. 69 (17) (1996), 2492.

[16]   J.S. Winslow, IEEE Trans. Consum. Electron. (1976), 318.

[17]   S.Y. Chou, P.R. Krauss, and P.J. Renstrom, Science, 272 (1996), 85.

[18]   B.D. Terris, H.J. Mamin, M.E. Best, J.A. Logan, and D. Rugar, Appl. Phys. Lett. 69 (1996), 4262.

[19] Micro-Optics: Elements, systems and applications, edited by H.P. Herzig (Taylor & Francis, London, 1997).

[20] E. Bakke, R. Busch and W.L. Johnson, Appl. Phys. Lett. 67 (22) (1995), 3260.

[21] C.A.Angell, Science 267 (1995), 1924.

[22] M.J. Stefan, Akad. Wiss. Wien. Math.-Natur. Klasse. Abt. 2 69 (1874), 713.

[23] G.J. Diennes and H.F. Klemm, Appl. Phys. 17 (1946), 458.

[24] R. Busch and W.L. Johnson, Materials Science Forum, 269-272 (1998), 577.

[25] N.F. Kazakov, Diffusion Bonding of Materials, 1981 (in Russian).

[26] G.V. Samsonov, A.P. Burykina and O.V. Yevtushenko, Avtomaticheskaya svarka 10 (1966), 30 (in Russian).

[27] N.F. Kazakov, "Diffusion bonding in Vacuum", Mashinostroyeniye, (1968) (in Russian).

[28] N.F. Kazakov, Svarochnoye proizvodstvo 9 (1973), 48.

[29] N.F. Kazakov, "Diffusion bonding of materials", Mashinostroyeniye (1976) (in Russian).

[30] G.V. Konyushkov, G.V. Kolylov and N. Yu, "Diffusion bonding in electronics", edited by N.F. Kazakov, (1974) (in Russian).

[31] K.A. Kocherguin, "Pressure welding", Mashinostroyeniye (1972) (in Russian).

[32] W.L. Johnson, "Bulk Glass-Forming Metallic Alloys: Science and Technology", MRS Bulletin, (1992), 42.

[33] K. Knorr, M.P. Macht, K. Freitag, and H. Mehrer, Journal of Non-Crystalline Solids, 250-252 (1999), 669.

[34] E. Budke, P. Fielitz, M. P. Macht, . Naundorf, G. Frohberg, Def. Diff. Forum 143-147 (1997), 825.

[35] P. Fielitz, E. Budke, M.P. Macht, V. Naundorf, G. Frohberg, Verhandl. Der DPG 5 (1998), 823.

[36] H. Ehmler, A. Heesemann, K. Ratzke, F. Faupel, Phys. Rev. Lett. 80 (1998), 4919.

[37] L. Shadospeaker, M. Shah and R. Busch, Scripta Materialia 50 (2004), 1035.